First Eocene–Miocene anuran fossils from Peruvian Amazonia: insights into Neotropical frog evolution and diversity

Olivier Jansen, Raúl Orencio Gómez, Antoine Fouquet, Laurent Marivaux, Rodolfo Salas-Gismondi, Pierre-olivier Antoine

Papers in Palaeontology (https://doi.org/10.1002/spp2.1542)

First Eocene–Miocene anuran fossils from Peruvian Amazonia: insights into Neotropical frog evolution and diversity

by OLIVIER JANSEN[1]*, RAÚL ORENCIO GÓMEZ[2]*, ANTOINE FOUQUET[3], LAURENT MARIVAUX[4], RODOLFO SALAS-GISMONDI[5] *and* PIERRE-OLIVIER ANTOINE[4]

[1] Laboratoire Paléontologie Évolution Paléoécosystèmes Paléoprimatologie, Université de Poitiers, UMR CNRS 7262, F-86073 Poitiers, France; 0009-0003-8770-4915

[2] CONICET-Departamento de Biodiversidad y Biología Experimental, Facultad de Ciencias Exactas y Naturales, Universidad de Buenos Aires, Ciudad Universitaria, C1428EGA Buenos Aires, Argentina; raulorenciogomez@gmail.com; 0000-0002-6600-3787

[3] Laboratoire Évolution et Diversité Biologique, CNRS, F-31062 Toulouse, France; 0000-0003-4060-0281

[4] Laboratoire de Paléontologie, Institut des Sciences de l'Évolution de Montpellier, cc64, Université de Montpellier, CNRS, IRD, F-34095 Montpellier, France; 0000-0002-2882-0874 (Laurent Marivaux); 0000-0001-9122-1818 (Pierre-Olivier Antoine)

[5] Departamento de Paleontología de Vertebrados, Museo de Historia Natural–Universidad Nacional Mayor San Marcos, Avenida Arenales 1256, Lima 11, Peru; 0000-0001-9990-8841

*Corresponding authors

Abstract: Anurans are one of the most diverse vertebrate groups, particularly in Amazonia, where species richness exceeds that of anywhere else. Amazonian frogs belong to three main lineages (Hyloidea, Microhylidae, and Pipidae), each of which has diversified during the Cenozoic. However, due to the virtual absence of anuran fossil record in that area, the evolutionary history of modern lineages has so far remained only accessible via molecular data. During the last decades, a series of field campaigns in Peruvian Amazonia led to the discovery of an unparalleled set of anuran bone fragments, scattered across different sites spanning the Eocene–Miocene time interval. We describe here these first Palaeogene and early Neogene anurans from Peru with a focus on humeral and ilial morphology, identifying five humeral and five ilial morphotypes. Humeral morphotypes suggest the presence of different lineages of Brachycephaloidea in Peruvian fossil assemblages, whereas ilial morphotypes suggest the presence of Leptodactylidae, although leptodactylid-like ilia also occur in some extant brachycephaloids. Pipids were also identified based on both humeral and ilial fragments. This study fills a major temporal and geographical gap in the evolutionary history of South American anurans, further revealing a lack of knowledge in the skeletal morphology of extant anuran families, as well as their inter- and intra- specific variability.

Key words: Anura, Amazonia, Brachycephaloidea, Eocene–Miocene, fossil, Pipidae

THE NEOTROPICS harbour an exceptional diversity of frogs compared to any other regions on the planet and particularly so in Amazonia (Jenkins *et al.* 2013; Vacher *et al.* 2020). Around 600 described species have been reported in this region, but molecular data suggest it represents a vast underestimation since the actual species richness might in fact be four or five times higher (Vacher *et al.* 2020). The Neotropical anuran fauna is composed of three main lineages (Hyloidea, Microhylidae, and Pipidae). Hyloidea account for 54% of extant neobatrachians and 81% of Neotropical species, whereas about one-fifth of Neotropical anurans belong to Microhylidae (Frost 2022*a*). Among hyloids, species of or close to Brachycephaloidea are expected to appear early as fossils in Amazonia as this diverse clade (>1,200 extant species; Frost 2022) probably originated and diversified from the early Palaeogene onward (Feng *et al*. 2017; Hime *et al*. 2021), although their fossil record is restricted to the Caribbean (e.g. Blackburn *et al.* 2020). Pipidae, an 'archeobatrachian' family of frogs known from Africa and South America, has a biogeographical history that was heavily influenced by the breakup of the Gondwana (Báez & Pugener 2003; Gómez 2016; Feng *et al*. 2017). In the Neotropics, pipids are currently represented by a single genus (*Pipa*) and seven nominal species (Fouquet *et al.* 2022*a*), but were much more diverse in the past as evidenced by a relatively rich fossil record that dates back to the Cretaceous (Báez *et al.* 2021; Barcelos & dos Santos 2022; Suazo Lara & Gómez 2022). The fossil record of *Pipa*, however, is still very limited and restricted to a few bones from the upper Miocene Solimões Formation of Brazil (Muniz *et al*. 2022) and upper Miocene Urumaco and upper Pliocene San Gregorio formations of Venezuela (Delfino & Sánchez-Villagra 2018; Carrillo-Briceño *et al.* 2021). Ranidae are also present in the Neotropics but dispersed into the region much later, around 8 Mya (million years ago) from Central America (Bossuyt *et al*. 2006; Wiens *et al*. 2009). Hyloidea and Microhylidae originated in the early Cretaceous and experienced a rapid diversification in the South American continent just after the K-Pg (Cretaceous-Palaeogene) mass extinction (Feng *et al*. 2017; Hime *et al*. 2021). The rapid diversification of frogs at the K-Pg suggests that this extinction may have triggered an explosive radiation among frogs due to an increase of available ecological opportunities (Roelants *et al.* 2007; Feng *et al.* 2017).

Even though the Neotropics possess one of the world's richest frog communities, the anuran fossil record is very scarce (Barcelos & dos Santos 2022), and restricted to few lineages coming from several sites mainly scattered across Patagonia and extra-Amazonian regions (e.g. Báez *et al*. 2009; Turazzini *et al*. 2016; Pérez-Ben *et al*. 2019; Gómez & Turazzini 2021; Suazo Lara & Gómez 2022; Turazzini & Gómez 2023*a*). Except for the recent description of fossils of two anuran species in fluvio-lacustrine settings of the Solimões Formation (Late Miocene of Acre, Brazilian Amazonia; Muniz *et al*. 2022), anurans are absent from the fossil record of Amazonia. This could result partly from the acidic soil conditions and the ephemeral nature of fossiliferous deposits due to frequent seasonal flooding (Antoine *et al.* 2016), as well as from the fragility of frog bones. The accessibility of those sites is furthermore hindered by the dense vegetation cover (Antoine *et al*. 2016). Due to the elusive fossil record of frogs in this region, their past diversity and their responses to Cenozoic climatic events remain largely unknown. Fossil anurans from Amazonia would be invaluable to better understand the evolutionary history of South American anurans, notably to improve divergence-time estimates of molecular phylogenies (Gómez 2016; Hime *et al*. 2021).

During the last decades, dozens of field campaigns have been undertaken in Peruvian Amazonia, leading to the discovery of around 120 anuran specimens in four sites spanning the late middle Eocene–Middle Miocene time interval (Antoine *et al*. 2016, 2021). These specimens are among the first fossil anurans ever discovered in Western Amazonia and as such, they are of high interest. They

consist of a majority of fragmentary postcranial remains and a few skull fragments. The objectives of this study were to identify and describe those specimens to better sketch the diversity and evolution of anurans of Western Amazonia during the mid-Cenozoic, and discuss their phylogenetic, palaeobiogeographical, and palaeoecological implications. CT-scan reconstructions of various South American extant taxa were used to allow meaningful comparisons of the specimens with extant species. Here we provide the description of the first Palaeogene and early Neogene fossil anurans from Peruvian Amazonia and report on a detailed morphological description of the humerus and ilia of relevant extant South American families. In addition, we discuss different sources of variability across both fossil and extant anuran species and their implication on the understanding of the evolutionary history of anurans in the Neotropics.

PALAEONTOLOGICAL AND GEOLOGICAL SETTINGS

The anuran fossils that were analysed come from twelve localities scattered across four scattered areas of Peruvian Amazonia (Contamana and Atalaya, Ucayali Basin; Tarapoto and Balsayacu, Huallaga Basin) mostly Palaeogene in age, with the exception of an Early Miocene locality and a late Middle Miocene one (Table 1, Fig. 1). These localities lie within the North Amazonian foreland basin, which originated from the Andean orogenesis (Hermoza *et al*. 2005; Roddaz *et al*. 2010; Antoine *et al*. 2016). Due to the tectonic movements associated with the Andean uplift, continuous sedimentary records from the Jurassic to the Holocene became exposed in a thick stratigraphic unit. In the last decades, the corresponding deposits have been intensely surveyed by a multidisciplinary team of researchers to improve the scant Cenozoic fossil record (e.g. Antoine *et al*. 2012, 2016, 2021; Boivin *et al*. 2017*a*, *b*, 2018, 2021, 2022; Marivaux *et al*. 2016, 2020).

Located in the Loreto Department, Peruvian Amazonia, the city of Contamana is bordered by the Fitzcarrald Arch in the NW and by the Ucayali River in the SW (Antoine *et al.* 2016) (Fig. 1A, B). Of the 34 fossil-bearing localities discovered in the area of Contamana along the Cachiyacu stream (a small affluent of the Ucayali River also referred as *Quebrada Cachiyacu*), only eight yielded anuran fossil remains (Fig. 1B). Five of those localities are assigned to the lower member of the Pozo Formation ("Pozo sands"), constituted by sediments from the late middle–late Eocene (CTA-27, CTA-29, CTA-47, CTA-51, and CTA-66; Antoine *et al*. 2016). For all these localities, the sediments suggest a freshwater environment consisting of low-energy small streams of fluvial origin even though dinoflagellate cysts in CTA-47 might support a marine influence (Antoine *et al*. 2016; Klaus *et al*. 2017). Anuran fossils were also discovered in two late Oligocene localities (CTA-32 and CTA-61), located at the base of the Chambira Formation, which overlays the variegated palaeosols and silts of the Lower Pozo Formation. CTA-61 at the base of the formation is characterised by conglomerates and sandbars suggesting a fluvial origin. In contrast, the grey-blue clays topping the conglomeratic channel of CTA-32 rather point to the steady waters of an oxbow lake (Antoine *et al*. 2016; Boivin *et al*. 2017*b*). Finally, CTA-63 is the only Miocene locality with anuran fossil specimens so far in the Contamana area. Located at the base of the Pebas Formation, this site is constituted by a 5m-thick sequence with blue silts showing herringbone cross-bedding, covered by laminated blue clays with millimetric leaf litters, and topped by a 2m-thick blue clay with pyrite nodules, ligneous wood, and litter. These deposits, assigned to the early Miocene, suggest a lacustrine environment with potential marine influence (Antoine *et al*. 2016).

Upstream in the Ucayali Basin, the TMB-01 locality, situated near Atalaya on *Río Tambo*, has yielded a single anuran specimen (Fig. 1A). Based on rodent and marsupial remains, a latest Eocene to earliest Oligocene age is provisionally proposed for this new locality, assigned to the upper member of the Pozo Formation. This outcrop is characterised by channelized reddish-bluish clays with pluri-millimetric limestone nodules, which correspond to fluvio-lacustrine settings.

Further north, in the Huallaga Basin, the San Martín Department hosts fossil localities south-east of the town of Tarapoto (TAR), and near the confluence of the *Río Mayo* and the *Río Huallaga* (Antoine *et al*. 2021) (Fig. 1A, C). Those localities span a late Eocene–Miocene interval with Miocene fluvial deposits restricted to the Juan Guerra area, notably along the *Río Mayo* (Marivaux *et al*. 2020; Boivin *et al.* 2021; Stutz *et al*. 2022). Those Miocene deposits have been associated with the lower member of the Ipururo Formation (Hermoza *et al*. 2005). In contrast, the Palaeogene section overhangs the confluence and provides a stratigraphical framework for the upper part of the Pozo Formation, which consists of shallow marine/littoral deposits, most probably spanning the late Eocene–late Oligocene interval (Roddaz *et al*. 2010; Antoine *et al*. 2016, 2021; Boivin *et al.* 2018). Among the dozen fossil-bearing localities discovered in that area, only three have yielded anuran remains. The early Oligocene TAR-01 locality consists of carbonate nodule-rich blue clays, whereas TAR-31 is a 10 to 15 cm-thick lens of microconglomerate dating from the late middle Miocene (Marivaux *et al*. 2020; Antoine *et al*. 2021; Boivin *et al.* 2021; Stutz *et al.* 2022) (Fig. 1C). Located in the vicinity of the village of Balsayacu (San Martín Department), along the *Río Huallaga*, the locality TAR-55 (Fig. 1A) has been assigned to the lower member of the Pozo Formation (late middle to late Eocene) (Assemat *et al*. 2019; Boivin *et al*. 2022). It is composed of poorly-consolidated microconglomerates including limestone nodules, soft pebbles and oxidised plant remains of fluvial to fluvio-deltaic origin.

MATERIAL AND METHODS

The sediments collected in the different localities were dried then screen-washed in river water using two sieves of different mesh sizes (2mm and 1mm, respectively). Medium-sized fossils (> 2mm) were collected by naked eye *in situ* while smaller fossils (between 1 and 2 mm) were sorted from the fine residues under stereomicroscopes during the field seasons (field laboratory) and the post-field seasons.

The fossil material consists of 122 specimens of millimetric dimensions with mostly fragmentary postcranial elements and a few cranial fragments. All the fossil specimens are permanently housed at the Vertebrate Palaeontology Department of the *Museo de Historia Natural of the Universidad Nacional Mayor San Marcos* (MUSM) in Lima, Peru. Those specimens have different preservation states and some display marks of acidic weathering. This material was scanned to obtain three-dimensional digital models of the fossils hence simplifying the manipulation and identification processes. Before the scan, the samples were separated by locality and placed in medicine pills filled with cotton wool. X-ray microtomography (µCT) was performed using a µCT-scanning station EasyTom 150/Rx Solutions with a resolution of 5 µm in the technical facilities of the Montpellier RIO Imaging (MRI) platform (ISEM, Université de Montpellier). The software Avizo 2019.1 was then used to isolate the different specimens in each pill. Each specimen was manually delimited and placed in independent label fields and the surface rendering module of Avizo was used to

reconstruct the surface with a smoothing value of 3. The software Morphodig v.1.6.7 (Lebrun 2018) was finally used to manipulate virtual objects.

Of the 122 specimens collected, humeral fragments were the most abundant with 42 distal ends identified, followed by radio-ulnae (25), ilia (16), and tibio-fibulae (16). A single ischium and a few pectoral (1 scapula, 5 coracoids), cranial (5), angulosplenial (1), and vertebral (4) fragments were also identified in the sample, but most of these are too fragmentary or poorly preserved and, at present, do not result informative of systematic affinities within Anura. Finally, the identification of six fossil specimens remained uncertain. Most of the fossil remains of frogs discovered are from the earliest interval (Eocene), especially from the locality CTA-27, which has yielded a wide morphological diversity within each skeletal unit (Fig. 2). In this work, we only focus on humeri and ilia as they are one of the most diagnostic bones, showing distinctive variation among the different anuran lineages (Roček *et al*. 2013; Gómez & Turazzini 2016; Blackburn *et al*. 2019, 2020; Keeffe & Blackburn 2020; Suazo Lara & Gómez 2022).

The comparative material comes from a combination of different sources. Available anatomical data and skeletons of a broad sample of South American anurans were first consulted to identify the skeletal bone and a hypothetical taxonomic identification for each specimen. At least one species of each modern family of frogs living in South America was then sampled (Table S1), except for Ranidae, which supposedly arrived later in South America (Bossuyt *et al*. 2006; Wiens *et al*. 2009). Ninety-nine species and 75 genera from 25 out of the 26 South American families were selected with an emphasis on brachycephaloid families. Ultimately, several genera and multiple species per genera were sampled for the most likely families with respect to the biogeography of current species and their evolutionary history as based on phylogenomic studies (Feng *et al*. 2017; Vasconcelos *et al*. 2019; Hime *et al*. 2021).

To build this database, CT-scans of modern species skeletons were downloaded from the platform Morphosource (https://www.morphosource.org/) with the prior approval of researchers and institutions in charge of those online collections (AMNH, CAS, CM, FMNH, KU, LCAM, MCZ, MVZ, RBINS- Scientific Heritage, UF, USNM, and YPM; see abbreviations below). For 31 species, selected based on the overall resemblance with the fossil material, the bone units of interest (humeri and ilia) were isolated with the software Avizo to allow an appropriate comparison for the articular surfaces of those bones.

Osteological terminology mainly follows that of Báez *et al*. (2012) and Gómez & Turazzini (2016, 2021) for ilial morphology, and those of Blackburn *et al*. (2019, 2020), Keeffe & Blackburn (2020) and Suazo Lara & Gómez (2022) for humeral morphology. Taxonomic arrangement mainly follows that of Feng *et al*. (2017), Hime *et al*. (2021), Motta *et al*. (2021), and Frost (2022). The terminology of Heinicke *et al*. (2018) is used in this paper for the phylogeny of Brachycephaloidea, separating the families Craugastoridae (Craugastorinae) and Strabomantidae (Hypodactylinae, Strabomantinae, Holoadeninae, and Pristimantinae). This suprageneric classification has also been used by Feng *et al*. (2017) and Motta *et al*. (2021). Due to the fragmentary nature of fossils and the uncertainty involved in the systematic assignments, we opt for the use of open taxonomic nomenclature following the recommendations of Bengston (1988).

In order to assess the comparative analysis, we built a character/taxon table with distinct character states as observed in the considered taxonomical sample (see Table S2). These descriptive features are designated hereunder between brackets, as follows (character number: character state).

Institutional abbreviations. AMNH, American Museum of Natural History, New York, NY, USA; CAS, California Academy of Sciences, San Francisco, CA, USA; CM, Carnegie Museum of Natural History, Pittsburgh, PA, USA; FMNH, Field Museum of Natural History (Zoology), Chicago, IL, USA; ISEM, Institut des Sciences de l'Évolution de Montpellier, Montpellier, France; KU, University of Kansas Biodiversity Institute, Lawrence, KS, USA; LCAM, Natural History Museums of Los Angeles County, Los Angeles, CA, USA; MCZ, Museum of Comparative Zoology, Harvard University, Cambridge, MA, USA; MUSM, Museo de Historia Natural of the Universidad Nacional Mayor San Marcos (Vertebrate Palaeontology Department), Lima, Peru; MVZ, Museum of Vertebrate Zoology, Berkeley Natural History Museums, Berkeley, CA, USA; RBINS, Scientific Heritage, Royal Belgian Institute of Natural Sciences, Scientific Survey of Heritage (SSH), Brussels, Belgium; UF, University of Florida, Florida Museum of Natural History, Gainesville, FL, USA; USNM, National Museum of Natural History, Smithsonian Institution, Washington, DC, USA; YPM, Yale Peabody Museum, Yale University, New Haven, CT, USA.

SYSTEMATIC PALAEONTOLOGY

Anuran fossil assemblages

We based the identification of different humeral and ilial morphotypes in the samples on distinctive morphological characteristics (Figs 3, 4). Morphotypes were used to account for the variability of the fossil remains without erecting potentially redundant biological taxa solely based on isolated bones, difficult to associate with each other (Roček *et al*. 2013). The variability between and within each morphotype was a major challenge in this study. Even if the specimens within each morphotype resemble each other overall, there is a lot of within- and between-group variation. The grouping in morphotypes remains therefore ambiguous since in this case, it is virtually impossible to distinguish among variability resulting from intra-specific variation processes such as individual ossification variation (Fabrezi & Goldberg 2009; Fabrezi *et al*. 2017; Ponssa *et al*. 2011; Barrionuevo 2020, Turazzini & Gómez 2023*b*), ontogenetic differences (Fabrezi & Goldberg 2009; Fabrezi *et al*. 2017; Gómez *et al.* 2017; Barrionuevo 2020), or sexual dimorphism (Lynch 1971; Duellman & Savitzky 1976; Ponssa & Medina 2016). This variability can also result from inter-specific or generic variation in plurispecific assemblages, due for instance to differential environmental adaptations (Heyer 1969*a*, 1969*b*; Emerson 1978; Jorgensen & Reilly 2013; Citadini *et al*. 2018; Keeffe & Blackburn 2020; Turazzini & Gómez 2023*b*), thereby suggesting that those morphotypes might represent different species or genera. The preservation status and the lack of knowledge on the inter- and intra- specific variation in extant species prevent us to choose between those possibly non-exclusive different hypotheses. The other humeral and ilial fossil remains that were not included in the different described morphotypes are not considered to correspond to those morphotypes because i) of their poor preservation status, hindering a relevant identification or ii) of their peculiar shape which might result from post-burial processes.

Distal humeral morphotypes

Among the 42 distal humeral fragments, four morphotypes were differentiated (Fig. 3). Those morphotypes were compared to extant South American frog families (Tables S1, S2; Fig. S1). Strongly-divergent humerus morphologies (large lateral and dorsal crests, projected epicondyles, small humeral balls) allowed certain families to be immediately discarded from the candidates (e.g. Bufonidae, Allophrynidae, Phyllomedusidae, or Hylidae). We emphasised the comparison on Ceuthomantidae, Eleutherodactylidae, Brachycephalidae, Craugastoridae, and Strabomantidae, as the fossil morphotypes from Peru possessed a combination of characters found in several of these brachycephaloid families.

AMPHIBIA Linnaeus, 1758
ANURA Fisher, 1813
NEOBATRACHIA Reig, 1958
BRACHYCEPHALOIDEA Günther, 1858
Family and Genus indet.

MORPHOTYPE 1

Material. Four fossil specimens were identified as documenting morphotype 1. Exemplar: MUSM 4746, MUSM 4747, and MUSM 4748 (Fig. 3); Other: MUSM 4749.

Localities. CTA-27 (Eocene).

Description. All the specimens regrouped within morphotype 1 correspond to distal humerus portions almost restricted to the humeral ball and the two epicondyles. Only MUSM 4748 shows the beginning of the diaphysis, which is ventrally bowed and has a deep ventral fossa (22:1). The humeral ball is rounded with an oblique fold slightly sigmoid on the lateral side in ventral view (4:0, 5:1). In lateral view, the humeral ball bears an inverted V-shaped depression below the enlarged distal end of the deep lateral epicondyle groove (17:1). The lateral epicondyle (=ectepicondyle = radial epicondyle) does not reach the distal margins of the humeral ball, and is pressed against the humeral ball (9:1, 10:0). In lateral, view the ectepicondyle forms a ridge (18:1). The medial epicondyle (=entepicondyle = ulnar epicondyle) is well developed, slightly projecting medially and extends until the distal margin of the humeral ball or slightly beyond (11:2, 12:1). In medial view, the distal extremity of the ulnar epicondylar crest epicondyle is convex and bears an oval depression (14:0, 15:1). Only visible on MUSM 4748, the medial epicondyle joins the diaphysis in a continuous manner (13:1), and both medial and lateral epicondylar crests are absent (20:0, 21:0).

Comparisons. Among the species compared, the round humeral ball with an oblique fold on the lateral side (4:0, 5:1), characteristic of morphotypes 1, is found in eleutherodactylids (but not in *Diasporus*, *Eleutherodactylus cuneatus*, and *E. karlschmidti*), brachycephalids (*Brachycephalus*), and strabomantids (*Oreobates* and *Noblella*) among brachycephaloids, and in leptodactylids (*Pleurodema* and *Edalorhina*) (Table S2; Fig. S1). The shape and orientation of this fold are, however, more similar to what is observed in species of *Phyzelaphryne*, *Adelophryne*,

Eleutherodactylus, and *Pleurodema*. Like morphotype 1, several species within Eleutherodactylidae have a medial epicondyle at the level or surpassing the distal margin of the round humeral ball, and slightly projected medially (11:2, 12:1). These characters are also present in *Craugastor*, *Edalorhina*, and some pipids. The inverted V-shaped depression (6:1) in lateral view is only shared by eleutherodactylids and *Pristimantis vinhai* (Strabomantidae), but its presence is unclear in *Phyzelaphryne*. A convex medial epicondyle (14:0) with an oval depression (15:1) is present in eleutherodactylids, but it has also been identified in *Craugastor, Oreobates*, and *Leptodactylus*. For *E. atkinsi*, the angular transition between the medial epicondyle and the diaphysis in medial view, as well as the length of the medial epicondyle, differ from morphotypes 1. A deep ventral fossa (22:1) and a deep lateral epicondylar groove with an enlarged end (17:1) are recovered in eleutherodactylids (except *Diasporus*, *E. cuneatus,* and *E. karlschmidti*), *Brachycephalus*, *Oreobates*, and *Edalorhina*. The specimen LACM 162445 (late early Oligocene, Puerto Rico) referred to as *Eleutherodactylus* sp. by Blackburn *et al*. (2020) is highly similar to morphotype 1, showing a long medial epicondyle and a round humeral ball with a sigmoid oblique fold.

MORPHOTYPE 2

Material. Morphotype 2 gathers six fossil specimens. Exemplar: MUSM 4755, MUSM 4756, and MUSM 4757 (Fig. 3); Others: MUSM 4752, MUSM 4753, and MUSM 4754.

Localities. CTA-27 and CTA-29 (Eocene), and CTA-61 (Oligocene).

Description. Morphotype 2 strongly resembles morphotype 1. Only MUSM 4757 shows parts of the diaphysis. Like morphotype 1, the diaphysis of morphotype 2 is ventrally oriented, bears a deep ventral fossa (22:1), and displays a smooth junction with the medial epicondyle. The overall shape of the humeral ball and the epicondyles are similar but a straight oblique fold in ventral view and a straight vertical lateral epicondyle (5:1, 19:2) differentiate morphotype 2 from 1.

Comparisons. As for morphotype 1, the round humeral ball with an oblique fold on the lateral side (4:0, 5:1) is found among the species compared in eleutherodactylids (but not in *Diasporus*, *E. cuneatus*, and *E. karlschmidti*), brachycephalids (*Brachycephalus*), and strabomantids (*Oreobates and Noblella*) among brachycephaloids, and in leptodactylids (*Pleurodema and Edalorhina*) (Table S2; Fig. S2). The shape and orientation of this fold are, however, more similar to what occurs in species of *Phyzelaphryne*, *Adelophryne*, *Eleutherodactylus,* and *Pleurodema*. Like morphotype 1 and 2, several species within Eleutherodactylidae have a medial epicondyle at the level or surpassing the distal margin of the round humeral ball, and slightly projected medially (11:2, 12:1). These characters are also present in *Craugastor*, *Edalorhina*, and some pipids. The inverted V-shaped depression (6:1) in lateral view is only shared with eleutherodactylids and *Pristimantis vinhai* (Strabomantidae), but its presence is unclear in *Phyzelaphryne*. A convex medial epicondyle (14:0) with an oval depression (15:1) is present in eleutherodactylids, but it has also been identified in *Craugastor, Oreobates*, and in *Leptodactylus*. For *Eleutherodactylus atkinsi*, the angular transition between the medial epicondyle and the diaphysis in medial view, as well as the length of the medial epicondyle, differ from morphotypes 1 and 2. A deep ventral fossa (22:1) and a deep lateral epicondylar groove with an enlarged end (17:1) are recovered in eleutherodactylids (except *Diasporus*, *Eleutherodactylus cuneatus*, and *E. karlschmidti*), *Brachycephalus*, *Oreobates*, and *Edalorhina*.

MORPHOTYPE 3

Material. Morphotype 3 is the most abundant morphotype among the samples as it corresponds to 17 humerus fragments. Exemplar: MUSM 4763, MUSM 4765, MUSM 4759, MUSM 4761, and MUSM 4766 (Fig. 3); Others: MUSM 4758, MUSM 4760, MUSM 4762, MUSM 4764, MUSM 4767, and MUSM 4768, MUSM 4769, MUSM 4770, MUSM 4771, MUSM 4772, MUSM 4773, and MUSM 4774.

Remark: Illustrated specimens (exemplar) have been used for both the description and comparison of morphotype 3. The other specimens were placed in that morphotype based on their resemblance with illustrated specimens, but a more precise analysis of their morphology would be required to verify their assignment to morphotype 3.

Localities. CTA-51, CTA-27, and CTA-66 (Eocene), CTA-61 and CTA-32 (Oligocene); CTA-63 and TAR-31 (Miocene).

Description. In morphotype 3, the distal portion of the diaphysis is relatively well preserved in several specimens. The diaphysis is bowed ventrally and separated from the humeral ball by a deep ventral fossa (22:1). The humeral ball is flattened on the lateral side, which gives an angular aspect of the humeral ball in ventral view (4:1). Medially, the humeral ball is rounded and downward oriented (7:0, 8:1). Both the medial and lateral epicondyles are poorly developed and restricted to about one-half of the humeral ball (9:0, 11:0). They are also poorly projected externally, generally closely appressed to the humeral ball, in the continuity of the diaphysis (10:0, 12:0). In medial view, the distal extremity of the medial epicondyle is concave (14:2), and a dorso-ventral constriction appears at the junction between the epicondyle and the diaphysis. In lateral view, the lateral epicondyle forms a thin ridge (18:1). The lateral epicondyle groove is deep with a V-shaped extremity and marked ridges in ventral view (17:2). There is no medial epicondylar crest, but a faint, thin lateral epicondylar crest is distinct (20:0, 21:1).

Comparisons. The peculiar humeral ball, ventrally angular (4:1) of morphotype 3 is only found, among the sampled taxa, in brachycephaloids such as ceuthomantids (*Ceuthomantis*), eleutherodactylids (*Eleutherodactylus karlschmidti*, and *E. cuneatus*), craugastorids (*Craugastor*), and *strabomantids* (*Barycholos*). The round downward-oriented humeral ball of morphotype 3 in medial view (7:0, 8:1) is uniquely recovered in *Barycholos* and *Tachiramantis* (Craugastoridae), as well as in pipids. *Ceuthomantis, E. cuneatus*, *E. karlschmidti*, *Barycholos*, *Niceforonia,* and *Strabomantis* haveshort medial and lateral epicondyles (9:0, 11:0) that are also not mediolaterally projecting in *Ceuthomantis* and *Niceforonia* (10:0, 12:0). A deep ventral fossa (22:1) and a deep lateral epicondylar groove with a V-shaped extremity and marked ridges (17:2) are recovered in ceuthomantids, eleutherodactylids (*E. cuneatus and E. karlschmidti*), craugastrodids (*Haddadus*), and in strabomantids (*Barycholos*, *Strabomantis*, and *Niceforonia*). Finally, the concave distal extremity of the medial epicondyle (14:2) present in morphotypes 3 is found in these species and in pipids (*P. pipa and P. snethlageae*).

MORPHOTYPE 4

Material. Morphotype 4 is documented by only one fossil specimen (MUSM 4775), which exhibits a well-preserved ventrally bowed diaphysis (Fig. 3).

Locality. CTA-27 (Eocene).

Description. The ventral fossa is particularly deep (22:1) and the humeral ball is angular (4:1), but it seems dorsoventrally crushed on the lateral side. In medial view, the humeral ball is oval and upward oriented (7:1, 8:2). The medial epicondyle is relatively short and poorly projected with a concave extremity (11:0, 12:0, 14:2). The lateral epicondyle is short (less than half of the humeral ball) and pressed on the humeral ball with a thin ridge on the lateral view (9:0, 10:0, 18:1). The lateral epicondylar groove is deep, with a V-shaped extremity (17:2). There is no medial epicondylar crest, whereas a faint, thin lateral epicondylar crest is distinct (20:0, 21:1).

Comparisons. The peculiar humeral ball, ventrally angular (4:1) of morphotype 4 is only found, among the sampled taxa, in brachycephaloids such as ceuthomantids (*Ceuthomantis*), eleutherodactylids (*Eleutherodactylus karlschmidti, and E. cuneatus*), craugastorids (*Craugastor)* and strabomantids *(Barycholos).* The oval upward-oriented humeral ball of morphotype 4 (7:1, 8:2) is shared by *Niceforonia*, *Haddadus*, *Ceuthomantis, Strabomantis*, *E. karlschmidti,* and *E. cuneatus*. Like morphotype 3 and 4, *Ceuthomantis*, *E. cuneatus*, *E. karlschmidti*, *Barycholos, Niceforonia* and *Strabomantis* have short medial and lateral epicondyles (9:0, 11:0), which are also not laterally projecting in *Ceuthomantis* and *Niceforonia* (10:0, 12:0). A deep ventral fossa (22:1) and a deep lateral epicondylar groove with a V-shaped extremity and marked ridges (17:2) are recovered in ceuthomantids, eleutherodactylids (*E. cuneatus* and *E. karlschmidti*), craugastrodids (*Haddadus*), and strabomantids (*Barycholos*, *Strabomantis*, and *Niceforonia*). Finally, the concave distal extremity of the medial epicondyle (14:2) present in both morphotypes 3 and 4, is also found in these brachycephaloid species and in pipids (*P. pipa and P. snethlageae*). However, when looking closer at the CTscan of *Barycholos pulcher* (uf:herp:68063), bone fragments in the surroundings of the humeral ball and epicondyles were noticed (Fig. 4), thereby suggesting that these elements were incompletely ossified. The angular shape of morphotypes 3 and 4 could therefore result from a difference in ossification or preservation of the humeral ball and epicondyles as these were found complete on another specimen of *B. pulcher* (uf:herp:68066). In this second specimen, the medial epicondyle is convex, possesses an oval depression, and reaches the distal margin of the humeral ball, whereas the lateral epicondyle is longer, pressed against the humeral ball, and lacks a V-shaped lateral epicondylar groove. Such characteristics resemble that of morphotype 1 & 2, other brachycephaloids, and also some leptodactylids.

XENOANURA Starrett, 1973
PIPIDAE Gray, 1825
cf. *Pipa* sp.

MORPHOTYPE 5

Material. Morphotype 5 is uniquely represented by MUSM 4776, which corresponds to a distal right humerus lacking the diaphysis (Fig. 3).

Locality. TMB-01 (Eocene-early Oligocene).

Description. Morphotype 5 is characterised by a small humeral ball (3:0), nested in a shallow ventral fossa (22:0). This humeral ball is rounded and downward oriented medially (4:0, 7:0, 8:1). The medial and lateral epicondyles are nearly symmetrically developed and both pressed against the humeral ball (10:0, 12:0) and moderately large as they do not surpass the distal margin of the humeral ball (9:1, 11:1), the lateral epicondyle being slightly longer than the medial epicondyle. The distal extremity of the medial epicondyle is convex and lacks an oval depression (14:0, 15:0), and the lateral epicondylar groove is shallow (17:0). Medial and lateral crests are absent in morphotype 5 (20:0, 21:0).

Comparisons. The combination of characters describing morphotype 5 is recovered in species of *Pipa* (Table S2; Fig. S1x). However, morphotype 5 differs from *Pipa aspera* in being less medio-laterally compressed and in having epicondyles of slightly different length, and also from "macropipa" species (i.e., *Pipa pipa and Pipa snethlageae*) in having shorter and rounded epicondyles lacking any points or crests (9:1, 11:1, 14:0). The small humeral ball and moderately large epicondyles (3:0, 9:1, 11:1) are also found in other pipids such as the Upper Cretaceous *Kuruleufenia* and the Palaeogene *Llankibatrachus* from Patagonia (Báez & Pugener 2003; Gómez 2016; Suazo Lara & Gómez 2022). However, morphotype 5 lacks the medial epicondylar crest (20:0) present in these extinct taxa. Also, morphotype 5 differs from *Kuruleufenia* in the medial epicondyle morphology, being distally rounded instead of sharply pointed, whereas it differs from *Llankibatrachus* in having epicondyles more symmetrically developed. Morphotype 5 is most similar to *Pipa parva* and *P. carvalhoi* in general proportions and epicondylar morphology.

Ilial morphotypes

The 17 ilium fragments recovered were also clustered into five morphotypes (Fig. 5). As for the humeral fossil remains, the ilial morphotypes identified here were compared with extant anuran species (Tables S1, S2; Fig. S2). Most dissimilar families were removed from candidates (e.g., Bufonidae, Allophrynidae, and Phyllomedusidae) based on the overall shape of the dorsal prominence, the acetabular fossa, the dorsal crest, and the ventral acetabular expansion. We emphasised the comparison on brachycephaloid families (Ceuthomantidae, Eleutherodactylidae, Brachycephalidae, Craugastoridae, and Strabomantidae) and Leptodactylidae as those morphotypes possessed a combination of characters found in multiple species of those families.

ANURA Fischer, 1813
NEOBATRACHIA Reig, 1958
BRACHYCEPHALOIDEA? Günther, 1858
Family and Genus indet.

MORPHOTYPE A

Material. Morphotype A is documented by three fossil specimens. MUSM 4790 is restricted to the dorsal prominence, the anterior part of the acetabulum and the beginning of the ilial shaft, which is more exposed in MUSM 4788 and even more in MUSM 4789. The latter also shows the dorsal acetabular expansion and the dorso-posterior wall of the acetabulum.

Locality. CTA-27 (Eocene).

Description. This morphotype is characterised by a moderately high dorsal prominence with steep concave anterior and posterior margins (26:1, 27:1). The apex of the dorsal prominence is approximately at the same level as the anterior margin of the acetabular fossa (29:1). The low dorsal prominence of MUSM 4789 (26:0) possesses irregular and flat margins suggesting a fracture. Morphotype A is also defined by a large dorsal crest developed as a flange, a deep supra-acetabular fossa preceding the dorsal prominence and a shallow dorsal crest depression between the anterior margin of the dorsal prominence and the ilial shaft (35:2, 44:1, 38:1). Even though the ventral acetabular expansion is poorly preserved, it appears to be ventromedially oriented and the most anterior margin of the pre-acetabular zone suggests a deep pre-acetabular fossa (45:1). On the lateral side, a proximal medial ridge ranges from the dorsal acetabular expansion to the beginning of the ilial shaft (47:1). The acetabular fossa is poorly delimited by a shallow rounded rim (49:1). As shown in MUSM 4790 and MUSM 4788, a quadrangular dorsal protuberance with a shallow depression projects dorsolaterally (31:3). The dorsal protuberance of MUSM 4790 possesses marked margins and a shallower depression. The dorsal acetabular expansion, only visible on MUSM 4789, is oriented posterodorsally (43:0).

Comparisons. A dorsal prominence with steep anterior and posterior margins (27:1) is only found in morphotypes A, *Pleurodema* and pipids. It is noteworthy that the steepness observed in morphotype A may result from the poor preservation of the dorsal crest and dorsal prominence margins. Moreover, as in morphotype A, a large dorsal crest (35:2) is present in leptodactylids (*Leptodactylus and Adenomera*), in multiple genera among Brachycephaloidea (except *Ceuthomantis*, *Diasporus*, *Pristimantis,* and *Niceforonia*), and in dendrobatids (*Ameerega*). However, only *Strabomantis*, *Brachycephalus*, *Haddadus*, *Barycholos*, *Leptodactylus* and *Ameerega* possess a supra-acetabular fossa associated with a dorsal crest depression (44:1, 38:1). The dorsolateral rectangular dorsal protuberance (31:3) of morphotype A is found in *Ceuthomantis*, *Eleutherodactylus* (except *Eleutherodacylus atkinsi*), *Brachycephalus*, *Strabomantis*, and *Leptodactylus.* The overall shape of the dorsal prominence, the supra-acetabular fossa and the dorsal protuberance with marked margins and a shallow depression of MUSM 4790, strongly resemble that of *Leptodactylus latrans* (Gómez *et al*. 2013). The fossil species *Leptodactylus* sp. (South American Pampas, Pliocene) described by Gómez *et al*. (2013) possesses the same features and is similar to the MUSM 4790 specimen.

MORPHOTYPE B

Material. Morphotype B, represented by a single fossil specimen. Exemplar: MUSM 4792 (Fig. 5).

Locality. CTA-27 (Eocene).

Description. Morphotype B is very similar to morphotype A but it differs in the larger size and more anterior position of the dorsal prominence and in the ventral acetabular expansion being oriented more ventrally. The anterior margin of the dorsal prominence is also higher while the dorsal crest, although dorsally broken, is more developed.

Comparisons. A dorsal prominence with steep anterior and posterior margins (27:1) is found in morphotype B, which is similar to morphotype B, *Pleurodema* and pipids. Even though a dorsal prominence of intermediate size is rather common in the studied taxa, only morphotype B, *Pleurodema* and pipids possess a very high dorsal prominence (26:2). Moreover, as in morphotype A and B, a large dorsal crest (35:2) is present in leptodactylids (*Leptodactylus and Adenomera*), in multiple genera among Brachycephaloidea (except *Ceuthomantis*, *Diasporus*, *Pristimantis,* and *Niceforonia*), and in dendrobatids (*Ameerega*). However, only *Strabomantis*, *Brachycephalus*, *Haddadus*, *Barycholos*, *Leptodactylus* and *Ameerega* possess a supra-acetabular fossa associated with a dorsal crest depression (44:1, 38:1). The dorsolateral rectangular dorsal protuberance (31:3) of morphotype A is found in *Ceuthomantis, Eleutherodactylus karlschmidti, Eleutherodactylus richmondi*, *Pleurodema*, *Strabomantis*, *Leptodactylus*, and in pipids. The overall shape of the dorsal prominence, the supra-acetabular fossa, the dorsal protuberance with marked margins and a shallow depression of MUSM 4790, strongly resemble the conditions observed in *Leptodacylus latrans* (Gómez *et al*. 2013). The fossil species *Leptodactylus* sp. (South American Pampa, Pliocene) described by Gómez *et al*. (2013) possesses the same features and is similar to the MUSM 4790 specimen.

MORPHOTYPE C

Material. Morphotype C is documented by two specimens limited to the most anterior portion of the acetabular fossa and the proximal section of the ilial shaft (MUSM 4793 and MUSM 4794; Fig. 5). Both lack the dorsal prominence and the ventral acetabular expansion due to poor preservation status.

Locality. CTA-27 (Eocene).

Description. A large dorsal crest forms a flange, but a dorsal crest depression is absent (35:2, 38:0). MUSM 4793 possesses a deep pre-acetabular fossa (45:1), lacking in MUSM 4794, but it might be due to poor preservation of the anterior margin of the acetabular rim. The proximal medial ridge is slightly marked, possibly because the anterior section is not preserved (47:1).

Comparisons. The preservation status of morphotype C hinders a thorough comparison with extant taxa, but like morphotype A and B, its ilial shaft is characterised by a large dorsal crest (35:2) and a proximal medial ridge (47:1) also observed in leptodactylids (*Leptodactylus* and *Adenomera*), dendrobatids (*Ameerega*), pipids (*Pipa pipa*), and in multiple genera among Brachycephaloidea (except *Ceuthomantis*, *Tachiramantis*, *Pristimantis*, *Niceforonia*, and *Noblella*).

HYLIDAE? Rafinesque, 1815
Genus indet.

MORPHOTYPE D

Material. Morphotype D consists of a single fragment of ilium, truncated up to the most anterior portion of the acetabular fossa and the proximal section of the ilial shaft (MUSM 4795) (Fig. 5).

Locality. CTA-27 (Eocene).

Description. The dorsal prominence is very low, slightly higher than the dorsal edge of the ilial shaft, and bell-shaped with both anterior and posterior margins gently sloping (26:0, 27:0). In dorsal view, the dorsal prominence is inclined laterally (28:2) and its apex is approximately at the same level as the anterior margin of the acetabular fossa in lateral view (29:1). The relatively small and globose dorsal protuberance projects dorsolaterally (31:2). Even though the anterior margin of the ventral acetabular expansion is broken, the pre-acetabular zone is broad with a shallow pre-acetabular fossa (46:3, 45:0). In medial view, the proximal medial view is absent, but a shallow groove extends along the length of the fossil at the level of the junction between the dorsal prominence and the ilial shaft (47:0).

Comparisons. Compared to morphotype C, the preservation status of morphotype D still allowed relevant anatomical comparisons with extant taxa. The low and bell-shaped dorsal prominence (26:0, 27:0) of morphotype D is observed in *Pristimantis duellmani* and *Tachiramantis* among scored taxa, but is also present in other anurans, including several hylids (Chantell 1964; Gómez & Turazzini 2016; Turazzini & Gómez 2023*b*), whereas the position of the dorsal prominence approximately at the same level than the anterior margin of acetabular fossa and laterally inclined (28:2, 29:1) is found in craugastorids (*Tachiramantis)*, strabomantids (*Pristimantis duellmani*), dendrobatids (*Ameerega*), hylids (*Osteocephalus*), and leptodactylids (*Pleurodema*). Morphotype D is also characterised by a wide pre-acetabular zone extending towards the iliac shaft (46:3), a presumably derived feature typical of hylids (Chantell 1964; Gómez & Turazzini 2016; Turazzini & Gómez 2023*b*), but that has also been reported in some myobatrachids (Lynch 1971; Gómez & Turazzini 2016). A shallow pre-acetabular fossa (45:0) is as well observed in hylids, *Brachycephalus,* dendrobatids, and pipids.

XENOANURA Starrett, 1973
PIPIDAE Gray, 1825
cf. *Pipa* sp.

MORPHOTYPE E

Material. Morphotype E gathers two ilium fragments (MUSM 4796 and MUSM 4797; Fig. 5).

Localities. CTA-27, CTA-29 (Eocene).

Description. MUSM 4796 possesses a thin relatively high triangular dorsal prominence (26:1, 27:0). Its apex is located clearly posterior to the anterior margin of the acetabular fossa in acetabular view (29:0). The dorsal protuberance is inconspicuous on those specimens and so is the interilial scar (30:0, 40:0). The two specimens also lack dorsal crests and proximal medial ridges (35:0, 47:0), but a well-developed lateral oblique ridge is present laterally at the junction between the ilial shaft and the pre-acetabular zone (39:1). The acetabular fossa extends towards the ilial shaft and merges with the dorsal acetabular expansion (49:0). The pre-acetabular zone is narrow and hidden by the acetabular fossa (46:0) while the proximal medial ridge is absent (47:0).

Comparisons. Morphotype E is characterised by a relatively high triangular dorsal prominence with an apex posterior to the anterior margin of the acetabular fossa (26:1, 27:0, 29:0). This combination of features has only been observed in pipids (*Pipa* and *Kuruleufenia*, a xenopodimorph pipid from Upper Cretaceous deposits of Patagonia originally described by Gómez (2016)). Morphotype E differs from *Pipa parva* and *P. aspera* in having a lateral oblique ridge (39:1), which is also present in other species of *Pipa* and in *Kuruleufenia* (Gómez 2016; Suazo Lara & Gómez 2022). Morphotype E also shares with most species of *Pipa* an elongated acetabular fossa that merges with the dorsal acetabular expansion (49:0), an inconspicuous pre-acetabular zone in lateral view (46:0), and the lack of the proximal medial ridge on the ilial shaft (47:0), which is apparently only present in *P. snethlageae* among the species analysed.

DISCUSSION

Humeral fragments similar to species of Brachycephaloidea

Based on morphological comparisons with extant families of South American anurans, distal humeral fragments from Peru have affinities with brachycephaloid anurans, a hyperdiverse clade (>1,200 nominal species) of direct-developing frogs (Frost 2022). Despite their incredible diversity and recent phylogenomic analyses, the relationships between extant families and subfamilies of Brachycephaloidea are still uncertain because of some conflicts between phylogenies (e.g. Barrientos *et al*. 2021; Motta *et al*. 2021). The monophyly of Eleutherodactylidae and most relationships among the genera, however, remain relatively stable across those studies.

Humeral morphotypes 1 and 2 strongly resemble those of representatives of Eleutherodacylidae as they share multiple traits with *Eleutherodactylus atkinsi*, *E. richmondi*, *Phyzelaphryne,* and *Adelophryne*. Among those, they possess a round humeral ball with an oblique fold on the lateral side, formed by an inverted V-shaped depression and a large medial epicondyle reaching the distal margin of the humeral ball or extending beyond. The convex shape and the oval depression of the medial epicondyle in medial view also participates in the similarity between morphotype 1 and 2, and extant eleutherodactylids. Each of these characters can be independently observed in many other lineages such as leptodactylids (*Edalorhina* and *Pleurodema*), craugastorids (*Craugastor)* and strabomantids (*Oreobates* and *Noblella*), but their combination is likely unique to eleutherodactylids.

Available time-calibrated phylogenies and the palaeobiogeographical distribution of eleutherodactylid subfamilies can also contribute to narrowing down the taxonomical identification of morphotypes 1 and 2. The genus *Eleutherodactylus*, which contains more than 200 of the 237 nominal species of the family, is currently restricted to the Caribbean islands and to the Southern part of North America, while *Diasporus* only occurs in Central America and Chocó (Colombia) (Heinicke *et al*. 2007; Fouquet *et al*. 2012). In contrast, Phyzelaphryninae are found in Amazonia, south of the Amazon River and *Adelophryne* occurs throughout the Guiana Shield and the Atlantic Forest (Fouquet *et al*. 2012). The original split between Phyzelaphryninae and Eleutherodactylinae is estimated between 44.2 and 32.8 Ma, and is associated with dispersal of the latter from South America towards Middle America and the proto-Caribbean. The recent discovery of the first fossil of *Eleutherodactylus* in Puerto Rico dating from the late early Oligocene (~29 Ma) further supports the idea that the two lineages had already split at that time (Blackburn *et al*. 2019). Due to the biogeographical isolation of *Eleutherodacylus* linked to a dispersal event, this genus is not a likely candidate for the taxonomical assignment of morphotypes 1 and 2, even though they could correspond to stem Eleutherodactylinae lineages instead. A more likely scenario is that they belong to a stem phyzelaphrynine, considering their current continental distribution and their evolutionary history. The basal split between *Adelophryne* and *Phyzelaphryne* is dated back to the late Eocene-early Oligocene ~40–30 Ma; Fouquet *et al*. 2012). Considering the southern Amazonian distribution of *Phyzelaphryne*, the fossils studied here might be related to this genus. However, *Phyzelaphryne* most likely originated within the Brazilian Shield and only dispersed westward secondarily, after the demise of the Pebas System *ca*. 10 Mya (Fouquet *et al*. 2012). Therefore, morphotypes 1 and 2 could correspond to stem Phyzelaphryninae, occurring before or just after the split between *Phyzelaphryne* and *Adelophryne.* The age of the fossils and their relatively small size (distal humeral width between the two epicondyles < 2 mm in ventral view), further supports their potential identification as stem Phyzelaphryninae, which are typically quite small (SVL < 2 cm). However, a possible phylogenetic position as stem eleutherodactylids or as stem brachycephaloids cannot be excluded, since the features shared between these morphotypes and phyzelaphrynines could be plesiomorphic and this combination of humeral features could be present along the early branches of the brachycephaloid tree. Both scenarios are in agreement with phylogenetic analyses suggesting that the early diversification of brachycephloids took place in northern South America (e.g. Hedges *et al.* 2008; Heinicke *et al.* 2009, 2018).

Humeral morphotypes 3 and 4 also possess characteristics similar to what occurs in Craugastoridae (*Craugastor escoces*) and Strabomantidae (*Strabomantis anomalus*, *Barycholos pulcher*, and *Niceforonia araiodactyla*), such as an angular humeral ball, short medial and lateral epicondyles, a V-shaped extremity of the lateral epicondylar groove, and a concave medial epicondyle. Some of these traits were also found in some eleutherodactylids (*E. karlschmidti* and *E. cuneatus),* and in *Ceuthomantis.* However, two different specimens of *Barycholos pulcher* (uf:herp:68063 and uf:herp:68066) revealed differential morphology of the humeral ball and epicondyles (Fig. 4). The small and poorly projected epicondyles with concave and V-shaped margins recovered in both morphotype 3 and 4 could result from a difference in ossification, coming (for instance) from ontogenetic variation (older individuals having more skeletons; Fabrezi & Goldberg 2009; Ponssa *et al*. 2011; Gómez *et al*. 2017; Turazzini & Gómez 2023*b*). Consequently, uf:herp:68063 and uf:herp:68066 would correspond to juvenile and adult specimens, respectively. Such morphological differences could also derive from differential preservation of the skeleton. Pending further studies on ontogenetic variability and interspecific variation of humeral morphology

within brachycephaloids, the taxonomic assignment of morphotypes 3 and 4 remains uncertain.

Regardless of possible differential ossification processes, morphotype 3 especially resembles that of *Barycholos pulcher* based on its round downward-oriented humeral ball in medial view and the lack of both medial and lateral epicondylar crests. *Barycholos* (Holoadeninae) only contains two extant species (*B. pulcher* and *B. ternetzi*) restricted to the Pacific lowlands of Ecuador and Central Brazil, respectively (Lynch 1980; Motta *et al*. 2021, Frost 2022). Monophyly between *Barycholos*, the northern clade of the polyphyletic genus *Noblella* and the newly described genus *Bahius* has been recovered by recent molecular phylogenetic analyses (De la Riva *et al*. 2017; Reyes-Puig *et al*. 2019; Motta *et al*. 2021). The northern clade of *Noblella* is composed of species living in the northern Andes on the eastern and western Andean slopes of Colombia and Ecuador, but also in Peruvian Amazonia. The widespread distribution of the clade regrouping *Barycholos*, *Noblella* and *Bahius* suggests that distant biogeographical areas of South America were connected, and that the ancestors of this clade had a broad biogeographical range, and thus underwent extensive extinctions (Hedges *et al*. 2008; Reyes-Puig *et al*. 2019; Motta *et al*. 2021). Morphotype 3 collected in Western Amazonia could therefore represent stem Holoadeninae or basal members of this subfamily, but, as for morphotypes 1 and 2, a link with other brachycephaloid lineages cannot be excluded.

We found a similarity between the humeral morphotype 4 and the brachycephaloid genus *Ceuthomantis* based on the presence of an angular humeral ball in ventral view, and an oval upward-oriented humeral ball in medial view. These features are only shared by *Ceuthomantis* and some eleutherodactylids (*Eleutherodactylus karlschmidti and E. cuneatus*). Like *Ceuthomantis*, morphotype 4 also possesses short epicondyles that are not projecting mediolaterally. Those traits are found independently in multiple brachycephaloid taxa. *Ceuthomantis* corresponds to the earliest divergence of brachycephaloids (Heinicke *et al*. 2009, 2018; Feng *et al*. 2017; Motta *et al.* 2021). The resemblance of morphotype 4 with an early-divergent brachycephaloid taxon currently restricted to the Guiana Shield highlands (Barrio- Amorós, 2010) and the multiple trait similarities with multiple craugastorids and strabomantids suggests that morphotype 4 could represent a stem brachycephaloid, or an early-diverging lineage within the crown group.

A leptodactylid affinity for ilial fragments or leptodactylid-like ilium in brachycephaloids?

Ilial morphotypes A and B strongly resemble that of Leptodactylidae, especially *Leptodactylus* and *Adenomera,* and some brachycephaloids based on the overall shape of their dorsal prominence, their dorsolateral rectangular or tear-shaped dorsal protuberance, their well-developed dorsal crest, and the presence of a supra-acetabular fossa and a dorsal crest depression. With more than 80 species, the genus *Leptodactylus* thrives in South and Central America (Heyer 1969*a*). This genus is divided in five major groups that display a relatively low interspecific osteological variability regardless of their different ecological adaptations (Heyer 1969*a*, 1969*b*; Lynch 1971; Ponssa *et al*. 2011). Despite the relative uniformity among *Leptodactylus* ilia, the peculiar rectangular dorsal protuberance of morphotype A with marked margins and a shallow depression shows similarities with the *L. latrans* group and with the oldest fossil of *Leptodactylus* dating from the Pliocene (Gómez *et al*. 2013). The poor preservation of fossils within morphotype A and ambiguous interrelationships among early-diverging *Leptodactylus* lineages prevent more precise comparisons with other *Leptodactylus* groups (Gómez *et al*. 2013). According to phylogenomic studies, crown

Leptodactylus probably appeared during the late Eocene (Feng *et al.* 2017; Hime *et al*. 2021). With an Eocene age (CTA-27), Morphotypes A and B could therefore represent stem species of *Leptodactylus*. However, other genera of Leptodactylinae, such as *Adenomera* as well as non-included Leptodactylinae (*Hydrolaetare* and *Lithodytes*), could also represent potential candidates. It is noteworthy that leptodactylid-like ilia have been observed in brachycephaloid anurans such as *Haddadus, Barycholos, Strabomantis*, and *Brachycephalus.* Because of i) the high level of trait similarity between hyloid taxa, ii) the lack of synapomorphies between the families of this clade, and iii) the poor preservation of morphotypes A and B, they could either be placed within leptodactylids or brachycephaloids. Given the seemingly abundance of brachycephaloids in most humeral morphotypes and the absence of leptodactylids in those morphotypes, the second option (brachycephaloids) may eventually be considered more likely.

Pipids in the mid-Cenozoic Peruvian anuran fossil assemblage

Humeral morphotype 5 and ilial morphotype E both suggest the presence of pipids in the Peruvian anuran fossil assemblage of Eocene–Oligocene age, which is not surprising since pipids are known to inhabit South America since the Late Cretaceous (Gómez 2016; Suazo Lara & Gómez, 2022) and are currently present in Amazonia, represented by *Pipa*. Both the humeral and ilial fragments were highly similar to what is known in *Pipa*, largely predating previous fossil records of the genus from the Late Miocene of Brazil (Muniz *et al*. 2022) and upper Miocene–Pliocene deposits of Venezuela (Delfino & Sánchez-Villagra 2018; Carrillo-Briceño *et al.* 2021). The presence of Peruvian pipids at the Eocene–Oligocene interval agrees with a previous molecular analysis that has recently revealed that the diversification of the extant *Pipa* probably started during the Early Neogene (Fouquet *et al*. 2022*a*). Extant representatives of *Pipa* display two main phenotypes: “macropipa” i.e., large-sized fully aquatic species associated with large aquatic habitats (*P. pipa* and *P. snethlageae*), and “micropipa” i.e., small-sized species associated with smaller water bodies and having, yet being mostly aquatic, more terrestrial habits than “macropipa” forms. Phylogenetic relationships suggest that a “micropipa” phenotype represents the ancestral state and that “macropipa” evolved secondarily during the Late Miocene (Fouquet *et al*. 2022*a*), which agrees with the appearance of “macropipa” forms in the fossil record (Delfino & Sánchez-Villagra 2018; Muniz *et al*. 2022). Humeral morphotype 5 and ilial morphotype E morphologically and metrically match more “micropipa”, although having minor distinctions with extant species, and they further largely predate the hypothetical settlement of extant “macropipa”. Accordingly, specimens found in the Peruvian fossil record could likely correspond to “micropipa”. An exhaustive morphological comparison of those fossils with South American pipids from Palaeogene and Neogene sites is needed to provide a better taxonomic identification, which could in turn help to calibrate molecular phylogenies of pipids.

Peruvian anuran assemblages during the Eocene–Miocene

The majority of morphotypes comes from Contamana at the CTA-27 locality of late middle–late Eocene age, which has yielded the complete set of anuran groups and most morphotypes (Fig. 2).

Only morphotype 5 (pipid humerus) was not recovered at CTA-27, coming from the slightly younger TMB-01 locality of Late Eocene–Early Oligocene age. Therefore, pipids are restricted to the Eocene–Early Oligocene in our sample. Most brachycephaloid? morphotypes and the hylid? ilium are also restricted to the CTA-27 locality, but morphotypes 2 and 3 of brachycephaloid? affinities extend up to the Late Oligocene and Middle Miocene, respectively, co-occurring in CTA-27 and CTA-61 (Fig. 2). The high Eocene diversity of anurans with at least six different morphotypes recorded at Contamana, with only two of them being recorded in the same region after the Eocene–Oligocene transition (EOT) could represent a true signal of extinction, although taphonomic biases cannot be completely ruled out (Antoine *et al.* 2016). During the EOT, drastic climatic and biotic changes occurred worldwide including in Western Amazonia (Antoine *et al.* 2021), mainly linked to the formation of the Antarctic circumpolar current (Toumoulin *et al.* 2020) and a decrease in atmospheric CO_2 (Westerhold *et al.* 2020). These rapid changes could be responsible for many extinctions at a regional scale. Moreover, during the Oligocene–Miocene the region has also transformed drastically due to the Andean uplift (Hoorn *et al.* 2010), which had a huge effect in anuran evolution (e.g. De la Riva 2020; Fouquet *et al.* 2022*b*). Is is noteworthy that the extensive time span of nearly 10 Ma and 25 Ma of morphotypes 2 and 3, respectively, indicate that evolution of the represented lineages occurred with very little divergence of humeral morphology (i.e. morphological stasis; Eldrege & Gould 1972), in agreement with the general trend of conserved morphology in anurans (e.g. Handrigan & Wassersug 2007; Fouquet *et al.* 2021*b*). However, even though the evolution of limb morphology is linked to frog's main habitat or locomotor behaviour (e.g. Jorgensen & Reilly 2013; Citadini et al. 2018; Pérez-Ben *et al.* in press), a multitude of microhabitats and capabilities exist within each main category. Morphological differences can therefore be very subtle among closely related species, despite of having distinct microhabitats and forming clades being distributed throughout the continent from lowlands to highlands (e.g. Kok *et al.* 2020; Fouquet *et al.* 2021*a*, 2022*c*). Therefore, what appears as a single morphotype may in fact hide a diverse group of terrestrial frogs with distinct ecologies.

Putative habitats of Western Amazonian mid-Cenozoic anurans

Depositional environments of the concerned anuran-yielding localities are strictly aquatic (either fluvial, lacustrine, or fluvio-deltaic settings). Nevertheless, they do not necessarily coincide strictly with the habitats of these anurans, notably due to biasing accumulating agents, such as post-mortem waterborne transport (Antoine *et al*. 2016) or predation (e.g., through bird pellets; for rodents, see Boivin *et al*. 2017*a*, *b*, 2018; for marsupials, see Stutz *et al*. 2022). The recognition of digestion marks on several anuran bone fragments (see above) substantiates this possible bias. Most fossils found in association with the present specimens, however, have continental affinities (see Table 1), either aquatic (e.g., fish and Nymphaceae plants; Antoine *et al*. 2016, 2021), semi-aquatic (e.g., decapods, gharials, and caimans; Marivaux *et al*. 2020), terrestrial/fossorial (e.g., ungulates and some rodents; Boivin *et al*. 2019), or arboreal (e.g., other rodents, marsupials, and vines/epiphyte plants; Antoine *et al*. 2021; Boivin *et al*. 2022; Stutz *et al*. 2022). As for vegetational cover, available proxies attest to the presence of tropical rainforests in all Palaeogene sections (Antoine *et al*. 2016, 2021), with an increasing seasonal contrast in the Upper Pozo Formation at Shapaja (early Oligocene; Antoine *et al*. 2021). A certain environmental heterogeneity may be recorded, with both a forest under warm and moist conditions and drier habitats around the TAR-31 locality by mid-

Miocene times (Marivaux *et al*. 2020; Boivin *et al.* 2021; Stutz *et al*. 2022).

The presence of brachycephaloids is in line with the presence of a tropical forest. In fact, most Amazonian-lowland brachycephaloids are currently associated with *terra firme* habitat and "micropipa" (e.g., *P. aspera, P. arrabali*) to small water bodies generally within forests. Without surprise and in combination with previous findings (Antoine *et al*. 2016, 2021; Marivaux *et al*. 2020), these fossils advocate for a mosaic of aquatic and terrestrial habitats around the depositional areas.

CONCLUSION

The description of the first Palaeogene anuran fossils from Amazonia led to the recognition of a great morphological diversity within anuran fossil remains from Peruvian Amazonia in as much as five humeral morphotypes and five ilial morphotypes were identified. It suggests that anurans were already diverse in Western Amazonia during the mid-Cenozoic. The combination of features present in both humeral and ilial fragments suggests the presence of hyloid and pipid families. Most distal humeral fragments have traits more similar to those of species from the diverse superfamily Brachycephaloidea, whereas most ilial fragments seem closer to what is known in leptodactylids. Multiple convergences such as leptodactylid-like ilia within Brachycephaloidea and phylogenetic uncertainties within Brachycephaloidea, however, obscure the taxonomic identification of those fossil specimens. Moreover, two ilia and one humerus fragment are considered to belong to pipids, but complementary analyses are required to refine their taxonomic assignment. Nevertheless, our study provides the first morphological analysis of a unique and precious fossil material that fills a major temporal and geographical gap in the evolutionary history of South American anurans. This study also reveals that the skeletal morphology of extant anuran families, as well as their inter- and intra- specific variability, remain poorly documented. Morphological comparative studies are therefore needed to better understand this variability. A thorough phylogenetic analysis would also contribute to a better overview of the synapomorphies of hyloid lineages, which could in turn help to disentangle the conflicts within brachycephaloid families. Furthermore, this study justifies palaeontological campaigns in secluded places such as Amazonia where new field trips are needed to increase the coverage of the sampled fossil anuran diversity, and further our understanding of the evolutionary history of Neotropical anurans throughout the Cenozoic.

*Acknowledgements***.** We thank David Blackburn, Joseph Martinez and Emily M. Braker for allowing us to use their virtual collection of anurans, available on MorphoSource. We also thank David Blackburn for kindly accepting our numerous download requests on Morphosource. Moreover, we would like to thank Renaud Lebrun, Anne-Lise Charruault and Mehdi Mouana (ISEM, France) for their technical support with the µCT-scanning station, the software Avizo and Morphodig. The 3D data presented in this work were produced through the technical facilities of the Montpellier RIO Imaging (MRI) platform (ISEM, Univ. Montpellier, France) and of the LabEx CeMEB. We are indebted to our colleagues and friends François Pujos (IANIGLA-Mendoza, Argentina), Myriam Boivin (INECOA-Jujuy, Argentina), Narla Stutz (Univ. Fed. Rio Grande do Sul, Brazil; ISEM, France), Maëva Orliac and Sylvain Adnet (ISEM, France), Julia Tejada-Lara (MUSM, Peru; Caltech, USA), Aldo Benites-Palomino (MUSM, Peru; Univ. Zurich, Switzerland), Rafael Varas-Malca, Ali Altamirano, and Walter Aguirre-Diaz (MUSM, Peru), Francis Duranthon (Museum de Toulouse,

France), Darin F. Croft (Case Univ., USA), Guillaume Billet (MNHN Paris, France), and Johan Yans (Univ. Namur, Belgium) for their active contribution to the field efforts in Peruvian Amazonia over the past 15 years. We also thankfully acknowledge the contribution of the editors, A. Lemierre (*Muséum National d'Histoire Naturelle*, Paris, France), and an anonymous reviewer for their valuable comments and suggestions. This paper is dedicated to the memory of Jean-Claude Rage (MNHN Paris, France), for his unparalleled contribution to fossil anuran knowledge, including preliminary taxonomic assignments of some elements described here. This study is part of the ongoing EMERGENCE strategic project of the LabEx CEBA (*Centre d'Etude de la Biodiversité Amazonienne*; ANR-10-LABX-25-01), which aims to characterise the effects of the global cooling recorded at the Eocene-Oligocene transition in Western Amazonia. This work and the fieldwork were supported by the LabEx CEBA, the CNRS Eclipse 2, CNRS Paleo2 & Toulouse University SPAM programs, the Leakey Foundation, the National Geographic Society, and the *Institut des Sciences de l'Évolution de Montpellier*.

Author contributions. **Conceptualization** OJ, ROG, AF, LM; **Data Curation** OJ, ROG, LM; **Formal Analysis** OJ, ROG, AF; **Funding Acquisition** LM, RS-G, P-OA; **Investigation** OJ, ROG, AF, P-OA; **Methodology** OJ, ROG, AF; **Project Administration** LM, P-OA; **Resources** ROG, AF, LM, RS-G, P-OA; **Software** ROG, AF, LM; **Writing – Original Draft Preparation** OJ, ROG, AF, P-OA; **Writing – Review & Editing** OJ, ROG, AF, LM, RS-G, P-OA.

DATA ARCHIVING STATEMENT

Data for 3D models of fossils described in this study are available in MorphoMuseuM (https://doi.org/10.18563/journal.m3.210). Data for 3D models of the illustrated and coded modern Neotropical species are available in MorphoSource (Table S1).

Editor. David Button

SUPPORTING INFORMATION

Additional Supporting Information can be found online (https://doi.org/10.1002/spp2.1542):
Table S1. List of South American species used for comparison with the Peruvian fossils.
Table S2. Character matrix.
Table S3. Fossil CT-scan information.
Fig. S1. Humeri of extant neotropical anurans.
Fig. S2. Ilia of extant neotropical anurans.
Fig. S3. New characters.

REFERENCES

ANTOINE, P.-O., MARIVAUX, L., CROFT, D. A., BILLET, G., GANERØD, M., J ARAMILLO, C., MARTIN, T., ORLIAC, M. J., TEJADA, J., ALTAMIRANO, A. J., DURANTHON, F., FANJAT, G., ROUSSE, S. and SALAS GISMONDI, R. 2012. Middle Eocene rodents from Peruvian Amazonia reveal the pattern and timing of caviomorph origins and biogeography. *Proceedings of the Royal Society B*, **279**, 1319–1326.

ANTOINE, P.-O., ABELLO, M. A., ADNET, S., ALTAMIRANO SIERRA, A. J., BABY, P., BILLET, G., BOIVIN, M., CALDERÓN, Y., CANDELA, A., CHABAIN, J., CORFU, F., CROFT, D. A., GANERØD, M., JARAMILLO, C., KLAUS, S., MARIVAUX, L., NAVARRETE, R. E., ORLIAC, M. J., PARRA, F., PÉREZ, M. E., PUJOS, F., RAGE, J. C., RAVEL, A., ROBINET, C., RODDAZ, M., TEJADA-LARA, J. V., VÉLEZ-JUARBE, J., WESSELINGH, F. P. and SALAS-GISMONDI, R. 2016. A 60-million-year Cenozoic history of Western Amazonian ecosystems in Contamana, eastern Peru. *Gondwana Research*, **31**, 30–59.

ANTOINE, P.-O., SALAS-GISMONDI, R., PUJOS, F., GANERØD, M. and MARIVAUX, L. 2017. Western Amazonia as a hotspot of mammalian biodiversity throughout the Cenozoic. *Journal of Mammalian Evolution*, **24**, 5–17.

ANTOINE, P.-O., YANS, J., CASTILLO, A. A., STUTZ, N., ABELLO, M. A., ADNET, S., CUSTÓDIO, M. A., BENITES- PALOMINO, A., BILLET, G., BOIVIN, M., HERRERA, F., JARAMILLO, C., MÁRTINEZ, C., MORENO, F., NAVARRETE, R. E., NEGRI, F. R., PARRA, F., PUJOS, F., RAGE, J. C., RIBEIRO, A. M., ROBINET, C., RODDAZ, M., TEJADA-LARA, J. V., VARAS-MALCA, R., VENTURA SANTOS, R., SALAS-GISMONDI, R. and MARIVAUX, L. 2021. Biotic community and landscape changes around the Eocene–Oligocene transition at Shapaja, Peruvian Amazonia: Regional or global drivers? *Global Planetary Change*, **202**, 103512.

ASSEMAT, A., BOIVIN, M., MARIVAUX, L., PUJOS, F., BENITES-PALOMINO, A., SALAS-GISMONDI, R., TEJADA-LARA, J. V, VARAS-MALCA, R. M., NEGRI, F. R., RIBEIRO, A. M. and ANTOINE, P.-O. 2019. Restes inédits de rongeurs caviomorphes du Paléogène de la région de Juanjui (Amazonie péruvienne): systématique, implications macro-évolutives et biostratigraphiques. *Geodiversitas*, **41**, 699–730.

BÁEZ, A. M., MOURA, G. J. and GÓMEZ, R. O. 2009. Anurans from the Lower Cretaceous Crato Formation of northeastern Brazil: implications for the early divergence of neobatrachians. *Cretaceous Research*, **30**, 829–846.

BÁEZ, A. M., GÓMEZ, R. O. and TAGLIORETTI, M. L. 2012. The archaic ilial morphology of an enigmatic pipid frog from the upper Pleistocene of the South American pampas. *Journal of Vertebrate Paleontology*, **32**, 304–314.

BÁEZ, A. M., MUZZOPAPPA, P. and DE MOURA, G. J. B. 2021. The earliest records of pipimorph frogs from South America (Aptian, Crato Formaton, Brazil): A critical evaluation. *Cretaceous Research*, **121**, 104728.

BARCELOS, L. A. and DOS SANTOS, R. O. 2022. The lissamphibian fossil record of South America. *Palaeobiodiversity and Palaeoenvironments*, 1–65.

BARRIENTOS, L. S., STREICHER, J. W., MILLER, E. C., PIE, M. R., WIENS, J. J. and CRAWFORD, A. J. 2021. Phylogeny of terraranan frogs based on 2,665 loci and impacts of missing data on phylogenomic analyses. *Systematics and Biodiversity*, **19**, 818–833.

BARRIO-AMORÓS, C. L. 2010. A New *Ceuthomantis* (Anura: Terrarana: Ceuthomantidae) from Sarisariñama Tepui, Southern Venezuela. *Herpetologica*, **66**, 172–181.

BARRIONUEVO, S. 2020. Variation in the growth and development of the hind limbs in frogs of the genus *Telmatobius* (Anura: Telmatobiidae). *Journal of Morphology*, **281**, 1534–1546.

BENGTSON, P. 1988. Open nomenclature. *Palaeontology*, **31**, 223–227.

BLACKBURN, D. C., ROBERTS, L., VALLEJO-PAREJA, M. C. and STANLEY, E. L. 2019. First Record of the anuran family Rhinophrynidae from the Oligocene of Eastern North America. *Journal of Herpetology*, **53**, 316–323.

BLACKBURN, D. C., KEEFFE, R. M., VALLEJO-PAREJA, M. C. and VÉLEZ-JUARBE, J. 2020. The earliest record of Caribbean frogs: A fossil coquí from Puerto Rico. *Biology Letters*, **16**, 20190947.

BOIVIN, M., MARIVAUX, L., CANDELA, A. M., ORLIAC, M. J., PUJOS, F., SALAS-GISMONDI, R., TEJADA-LARA, J. V. and ANTOINE, P.-O. 2017*a*. Late Oligocene caviomorph rodents from Contamana, Peruvian Amazonia. *Papers in Palaeontology*, **3**, 69–109.

BOIVIN, M., MARIVAUX, L., ORLIAC, M., PUJOS, F., SALAS-GISMONDI, R., TEJADA-LARA, J. V. and ANTOINE, P.-O. 2017*b*. Late middle Eocene caviomorph rodents from Contamana, Peruvian Amazonia. *Palaeontologia Electronica*, **20**, 1–50.

BOIVIN, M., MARIVAUX, L., PUJOS, F., SALAS-GISMONDI, R., TEJADA-LARA, J. V., VARAS-MALCA, R., and ANTOINE, P.-O. 2018. Early Oligocene caviomorph rodents from Shapaja, Peruvian Amazonia. *Palaeontographica A*, **311**, 87–156.

BOIVIN, M., GINOT, S., MARIVAUX, L., ALTAMIRANO, A. J., PUJOS, F., SALAS-GISMONDI, R., TEJADA-LARA, J. V. and ANTOINE, P.-O. 2019. Tarsal morphology and locomotor adaptation of some late middle Eocene caviomorph rodents from Peruvian Amazonia reveal early ecological diversity. *Journal of Vertebrate Paleontology*, **38**, e1555164.

BOIVIN, M., MARIVAUX, L., AGUIRRE-DIAZ, W., BENITES-PALOMINO, A., BILLET, G., PUJOS, F., SALAS-GISMONDI, R., STUTZ, N. S., TEJADA-LARA, J. V., VARAS-MALCA, R., WALTON, A. H. and ANTOINE, P.-O. 2021. Late middle Miocene caviomorph rodents from Tarapoto, Peruvian Amazonia. *PLoS ONE*, **16** (11), e0258455.

BOIVIN, M., MARIVAUX, L., AGUIRRE-DIAZ, W., ANDRIOLLI CUSTÓDIO, M., BENITES-PALOMINO, A., PUJOS, F., RODDAZ, M., SALAS-GISMONDI, R., STUTZ, N., TEJADA-LARA, J. V., YANS, J. and ANTOINE, P.-O. 2022. Eocene caviomorph rodents from Balsayacu (Peruvian Amazonia). *Paläontologische Zeitschrift*, **96**, 135–160.

BOSSUYT, F., BROWN, R. M., HILLIS, D. M., CANNATELLA, D. C., MILINKOVITCH and M. C. 2006. Phylogeny and biogeography of a cosmopolitan frog radiation: Late Cretaceous diversification resulted in continent-scale endemism in the family Ranidae. *Systematic Biology*, **55**, 579–594.

CARRILLO-BRICEÑO, J. D., SÁNCHEZ, R., SCHEYER, T. M., CARRILLO, J. D., DELFINO, M., GEORGALIS, G. L., KERBER, L., RUIZ-RAMONI, D., BIRINDELLI, J. L., CADENA, E. A. and RINCÓN, A. F. 2021. A Pliocene-Pleistocene continental biota from Venezuela. *Swiss Journal of Palaeontology*, **140**, 1–76.

CHANTELL, C. J. 1964. Some Mio-Pliocene hylids from the Valentine Formation of Nebraska. *American Midland Naturalist*, **72**, 211–225.

CITADINI, J. M., BRANDT, R., WILLIAMS, C. R. and GOMES, F. R. 2018. Evolution of morphology and locomotor performance in anurans: relationships with microhabitat diversification. *Journal of Evolutionary Biology*, **31**, 371–381.

COHEN, K. M., FINNEY, S. C., GIBBARD, P. L. and FAN, J.-X. 2013; updated. The ICS International Chronostratigraphic Chart. *Episodes* **36**, 199–204.

DE LA RIVA, I. 2020. Unexpected beta-diversity radiations in highland clades of Andean Terraranae frogs. 741–764. *In* RULL, V. and CARNAVAL, A. (eds) *Neotropical diversification: Patterns and processes*. Fascinating life sciences. Springer, 820 pp.

DE LA RIVA, I., CHAPARRO, J. C., CASTROVIEJO-FISHER, S. and PADIAL, J. M. 2018. Underestimated anuran radiations in the high Andes: five new species and a new genus of Holoadeninae, and their phylogenetic relationships (Anura: Craugastoridae). *Zoological Journal of the Linnean Society*, **182**, 129–172.

DELFINO, M. and SÁNCHEZ-VILLAGRA, M. R. 2018. A late Miocene pipine frog from the Urumaco Formation, Venezuela. *Ameghiniana*, **55**, 210–214.

DUELLMAN, W. E. and SAVITZKY, A. H. 1976. Aggressive behavior in a centrolenid frog, with comments on territoriality in anurans. *Herpetologica*, **32**, 401–404.

ELDREDGE, N. and GOULD, S. J. 1972. Punctuated equilibria: an alternative to phyletic gradualism. 82–115. *In* SCHOPF, T. J. M. (ed.) *Models in paleobiology*. Freeman, Cooper, 250 pp.

EMERSON, S. B. 1978. Allometry and jumping in frogs: helping the twain to meet. *Evolution*, **32**, 551–564.

FABREZI, M. and GOLDBERG, J. 2009. Heterochrony during skeletal development of *Pseudisplatensis* (Anura, Hylidae) and the early offset of skeleton development and growth. *Journal of Morphology*, **270**, 205–220.

FABREZI, M., GOLDBERG, J. and CHULIVER PEREYRA, M. 2017. Morphological variation in anuran limbs:

constraints and novelties. *Journal of Experimental Zoology Part B: Molecular and Developmental Evolution*, **328**, 546–574.

FENG, Y.-J., BLACKBURN, D. C., LIANG, D., HILLIS, D. M., WAKE, D. B., CANNATELLA, D. C. and ZHANG, P. 2017. Phylogenomics reveals rapid, simultaneous diversification of three major clades of Gondwanan frogs at the Cretaceous–Paleogene boundary. *Proceedings of the national Academy of Sciences*, **114**, E5864–E5870.

FISCHER, G. 1813. *Zoognosia tabulis synopticis illustrata, in usum praelectionum Academiae Imperialis Medico-Chirurgicae Mosquensis edita*. *Volume 1*, Third edition. Nicolai Sergeidis Vsevolozsky, Moscow, i-xiv, 464 pp.

FOUQUET, A., LOEBMANN, D., CASTROVIEJO-FISHER, S., PADIAL, J. M., ORRICO, V. G. D., LYRA, M. L., ROBERTO, I. J., KOK, P. J. R., HADDAD, C. F. B. and RODRIGUES, M. T. 2012. From Amazonia to the Atlantic forest: molecular phylogeny of Phyzelaphryninae frogs reveals unexpected diversity and a striking biogeographic pattern emphasizing conservation challenges. *Molecular Phylogenetics and Evolution*, **65**, 547–561.

FOUQUET, A., LEBLANC, K., FRAMIT, M., RÉJAUD, A., RODRIGUES, M. T., CASTROVIEJO-FISHER, S., PELOSO, P. L. V., PRATES, I., MANZI, S., SUESCUN, U., BARONI, S., MORAES, L. J. C. L., RECODER, R., DE SOUZA, S. M., DAL VECCHIO, F., CAMACHO, A., GHELLERE, J. M., ROJAS-RUNJAIC, F. J. M., GAGLIARDI-URRUTIA, G., DE CARVALHO, V. T., GORDO, M., MENIN, M., KOK, P. J. R., HRBEK, T., WERNECK, F. P., CRAWFORD, A. J., RON, S. R., MUESES-CISNEROS, J. J., ROJAS ZAMORA, R. R., PAVAN, D., IVO SIMÕES, P., ERNST, R. and FABRE, A. C. 2021*a*. Species diversity and biogeography of an ancient frog clade from the Guiana Shield (Anura: Microhylidae: *Adelastes*, *Otophryne*, *Synapturanus*) exhibiting spectacular phenotypic diversification. *Biological Journal of the Linnean Society*, **132**, 233–256.

FOUQUET, A., LEBLANC, K., FABRE, A. C., RODRIGUES, M. T., MENIN, M., COURTOIS, E. A., DEWYNTER, M., HÖLTING, M., ERNST, R., PELOSO, P. and KOK, P. J. 2021*b*. Comparative osteology of the fossorial frogs of the genus *Synapturanus* (Anura, Microhylidae) with the description of three new species from the Eastern Guiana Shield. *Zoologischer Anzeiger*, **293**, 46–73.

FOUQUET, A., CORNUAULT, J., RODRIGUES, M. T., WERNECK, F. P., HRBEK, T., ACOSTA-GALVIS, A. R., MASSEMIN, D., KOK, P. J. R. and ERNST, R. 2022*a*. Diversity, biogeography, and reproductive evolution in the genus *Pipa* (Amphibia: Anura: Pipidae). *Molecular Phylogenetics and Evolution*, **170**, 107442.

FOUQUET, A., RÉJAUD, A., RODRIGUES, M. T., RON, S. R., CHAPARRO, J. C., OSORNO, M., WERNECK, F. P., HRBEK, T., LIMA, A. P., CAMACHO-BADANI, T., JARAMILLO, A. F. and CHAVE, J. 2022*b*. Diversification of the *Pristimantis conspicillatus* group (Anura: Craugastoridae) within distinct neotropical areas throughout the Neogene. *Systematics and Biodiversity*, **20**, 1–16.

FOUQUET, A., PELOSO, P., JAIRAM, R., LIMA, A. P., MÔNICO, A. T., ERNST, R. and KOK, P. J. R. 2022*c*. Back from the deaf: Integrative taxonomy confirms a new species of *Pristimantis* Jiménez de la Espada, 1870 (Anura, Strabomantidae) endemic to the eastern Guiana Shield and revalidates *Hylodes grandoculis* van Lidth de Jeude, 1904. *Organisms Diversity and Evolution*, **22**, 1065–1098.

FROST, D. R. 2022. Amphibian Species of the World: an Online Reference. Version 6.1 (25/05/2022). https://amphibiansoft heworld.amnh.org/index.php

GÓMEZ, R. O. 2016. A new pipid frog from the Upper Cretaceous of Patagonia and early evolution of crown-group Pipidae. *Cretaceous Research*, **62**, 52–64.

GÓMEZ, R. O. and TURAZZINI, G. F. 2016. An overview of the ilium of anurans (Lissamphibia, Salientia), with a critical appraisal of the terminology and primary homology of main ilial features. *Journal of Vertebrate Paleontology*, **36**, e1030023.

GÓMEZ, R. O. and TURAZZINI, G. F. 2021. The fossil record and phylogeny of South American horned frogs (Anura, Ceratophryidae). *Journal of Systematic Palaeontology*, **19**, 91–130.

GÓMEZ, R. O., PÉREZ-BEN, C. M. and STEFANINI, M. I. 2013. Oldest record of *Leptodactylus* Fitzinger, 1826 (Anura, Leptodactylidae), from the early Pliocene of the South American Pampas. *Journal of Vertebrate Paleontology*, **33**, 1321–1327.

GÓMEZ, R. O., REGUEIRA, E., O'DONOHOE, M. A. and HERMIDA, G. N. 2017. Delayed osteogenesis and calcification in a large true toad with a comparative survey of the timing of skeletal ossification in anurans.

Zoologischer Anzeiger, **267**, 101–110.

GRAY, J. E. 1825. A synopsis of the genera of reptiles and Amphibia, with a description of some new species. *Annals of Philosophy, New Series*, 10, 193–217.

GÜNTHER, A. C. L. G. 1858. Neue Batrachier in der Sammlung des britischen Museums. Archiv für Naturgeschichte, **24**, 319–328.

HALVORSEN, K. A. T. 2010. Time since divergence between the blue whiting sister species *Micromesistius poutassou* and *M. australis.* Unpublished Master's thesis, Norges teknisk-naturvitenskapelige universitet, Fakultet for naturvitenskap og teknologi, Institutt for biologi.

HANDRIGAN, G. R. and WASSERSUG, R. J. 2007. The anuran Bauplan: a review of the adaptive, developmental, and genetic underpinnings of frog and tadpole morphology. *Biological Reviews*, **82**, 1–25.

HEDGES, S. B., DUELLMAN, W. E. and HEINICKE, M. P. 2008. New World direct-developing frogs (Anura: Terrarana): molecular phylogeny, classification, biogeography, and conservation. *Zootaxa*, **1737**, 1– 182.

HEINICKE, M. P., DUELLMAN, W. E. and HEDGES, S. B. 2007. Major Caribbean and Central American frog faunas originated by ancient oceanic dispersal. *Proceedings of the National Academy of Sciences*, **104**, 10092–10097.

HEINICKE, M. P., DUELLMAN, W. E., TRUEB, L., MEANS, B. D., MACCULLOCH, R. D. and HEDGES, S. B. 2009. A new frog family (Anura: Terrarana) from South America and an expanded direct-developing clade revealed by molecular phylogeny. *Zootaxa*, **2211**, 1–35.

HEINICKE, M. P., LEMMON, A. R., LEMMON, E. M., MCGRATH, K. and HEDGES, S. B. 2018. Phylogenomic support for evolutionary relationships of New World direct-developing frogs (Anura: Terraranae). *Molecular phylogenetics and evolution*, **118**, 145–155.

HERMOZA, W., BRUSSET, S., BABY, P., GIL, W., RODDAZ, M., GUERRERO, N. and BOLAÑOS, M. 2005. The Huallaga foreland basin evolution: thrust propagation in a deltaic environment, northern Peruvian Andes. *Journal of South American Earth Sciences*, **19**, 21–34.

HEYER, W. R. 1969*a*. Studies on the genus *Leptodactylus* (Amphibia, Leptodactylidae). 3. A redefinition of the genus *Leptodactylus* and a description of a new genus of Leptodactylid frogs. *Contributions in Science, Natural History Museum of Los Angeles County*, **155**, 1–14.

HEYER, W. R. 1969*b*. The adaptive ecology of the species groups of the genus *Leptodactylus* (Amphibia, Leptodactylidae). *Evolution*, **23**, 421–428.

HIME, P. M., LEMMON, A. R., MORIARTY LEMMON, E. C., PRENDINI, E., BROWN, J. M., THOMSON, R. C., KRATOVIL, J. D., NOONAN, B. P., ALEXANDER PYRON, R., PELOSO, P. L. V., KORTYNA, M. L., SCOTT KEOGH, J., DONNELLAN, S. C., MUELLER, R. L., RAXWORTHY, C. J., KUNTE, K., RON, S. R., DAS, S., GAITONDE, N., GREEN, D. M., LABISKO, J., CHE, J. and WEISROCK, D. W. 2021. Phylogenomics reveals ancient gene tree discordance in the amphibian tree of life. *Systematic Biology*, **70**, 49–66.

HOORN, C., WESSELINGH, F. P., ter STEEGE, H., BERMUDEZ, M. A., MORA, A., SEVINK, J., SANMARTIN, I., SANCHEZ- MESEGUER, A., ANDERSON, C. L., FIGUEIREDO, J. P. and JARAMILLO, C. 2010. Amazonia through time: Andean uplift, cli-mate change, landscape evolution, and biodiversity. *Science*, **330**, 927–931.

JANSEN, O., GÓMEZ, R. O., FOUQUET, A., MARIVAUX, L., SALAS-GISMONDI, R. and ANTOINE, P.-O. 2023. 3D models related to the publication: First Eocene-Miocene anuran fossils from Peruvian Amazonia: insights into Neotropical frog evolution and diversity. *MorphoMuseuM* **9**, e210. https://doi.org/10.18563/journal.m3.210

JENKINS, C. N., PIMM, S. L. and JOPPA, L. N. 2013. Global patterns of terrestrial vertebrate diversity and conservation. *Proceedings of the National Academy of Sciences of the United States of America*, **110**, 2603–2610.

JORGENSEN, M. E. and REILLY, S. M. 2013. Phylogenetic patterns of skeletal morphometrics and pelvic traits in relation to locomotor mode in frogs. *Journal of Evolutionary Biology*, **26**, 929–943.

KEEFFE, R. and BLACKBURN, D. C. 2020. Comparative morphology of the humerus in forward-burrowing frogs. *Biological Journal of the Linnean Society*, **131**, 291–303.

KLAUS, S., MAGALHÃES, C., SALAS-GISMONDI, R., GROSS, M. and ANTOINE, P.-O. 2017. Palaeogene and

Neogene brachyurans of the Amazon Basin: a revised first appearance date for primary freshwater crabs (Brachyura, Trichodactylidae). *Crustaceana*, **90**, 953–967.

KOK, P.J., VAN DER VELDEN, M. A., MEANS, D. B., RATZ, S., JOSIPOVIC, I., BOONE, M. and MCDIARMID, R. W. 2020. Coping with the extremes: comparative osteology of the tepui-associated toad *Oreophrynella* and its bearing on the evolution of osteological novelties in the genus. *Zoological Journal of the Linnean Society*, **190**, 114–139.

LEBRUN, R. 2018. MorphoDig, an open-source 3D freeware dedicated to biology. *In IPC5 The 5th International Palaeontological Congress*. Available at https://morphomuseum.com/downloadMorphodig

LYNCH, J. D. 1971. Evolutionary relationships, osteology and zoogeography of leptodactyloid frogs. *University of Kansas publications, Museum of Natural History, Miscellaneous Publications*, **53**, 1–238.

LYNCH, J. D. 1980. A new species of *Barycholos* from Estado Goias, Brasil (Amphibia, Anura, Leptodactylidae) with remarks on related genera. B*ulletin du Muséum National d'Histoire Naturelle*, **2**, 289–302.

MARIVAUX, L., ADNET, S., ALTAMIRANO-SIERRA, A. J., BOIVIN, M., PUJOS, F., RAMDARSHAN, A., SALAS-GISMONDI, R., TEJADA-LARA, J. V. and ANTOINE, P.-O. 2016. Neotropics provide insights into the emergence of New World monkeys: new dental evidence from the late Oligocene of Peruvian Amazonia. *Journal of Human Evolution*, **97**, 159–175.

MARIVAUX, L., AGUIRRE-DIAZ, W., BENITES-PALOMINO, A., BILLET, G., BOIVIN, M., PUJOS, F., SALAS-GISMONDI, R., TEJADA-LARA, J. V., VARAS-MALCA, R. M. and ANTOINE, P. -O. 2020. New record of *Neosaimiri* (Cebidae, Platyrrhini) from the late Middle Miocene of Peruvian Amazonia. *Journal of Human Evolution*, **146**, 102835.

MOTTA, A. P., TAUCCE, P. P. G., HADDAD, C. F. B. and CANEDO, C. 2021. A new terraranan genus from the Brazilian Atlantic Forest with comments on the systematics of Brachycephaloidea (Amphibia: Anura). *Journal of Zoological Systematics and Evolutionary Research*, **59**, 663–679.

MUNIZ, F. P., BISSARO-JÚNIOR, M. C., GUILHERME, E., SOUZA-FILHO, J. P. D., NEGRI, F. R. and HSIOU, A. S. 2022. Fossil frogs from the upper Miocene of southwestern Brazilian Amazonia (Solimões Formation, Acre Basin). *Journal of Vertebrate Paleontology*, **41**, e2089853.

PÉREZ-BEN, C. M., TURAZZINI, G. F. and GÓMEZ, R. O. 2019. A Last Glacial anuran assemblage from the inland Pampas of South America provides insights into climate and environments during Marine Isotope Stage 3. *Journal of Vertebrate Paleontology*, **39**, e1627365.

PÉREZ-BEN, C. M., LIRES, A. I. and GÓMEZ, R. O. Frog limbs in deep time: is jumping locomotion at the roots of the anuran Bauplan? *Paleobiology,* published online 15 September. https://doi.org/10.1017/pab.2023.23

PONSSA, M. L. and MEDINA, R. G. 2016. Comparative morphometrics in leptodactyline Frogs (Anura, Leptodactylidae, Leptodactylinae): does burrowing behavior relate to sexual dimorphism? *Journal of Herpetology*, **50**, 604–615.

PONSSA, M. L., BRUSQUETTI, F. and SOUZA, F. L. 2011. Osteology and intraspecific variation of *Leptodactylus podicipinus* (Anura: Leptodactylidae), with comments on the relationship between osteology and reproductive modes. *Journal of Herpetology*, **45**, 79–93.

RAFINESQUE, C. S. 1815. *Analyse de nature, ou Tableau de l'universe et des corps organisés*. Jean Barravecchia, Palermo.

REIG, O. A. 1958. Proposiciones para una nueva macrosistematica de los anuros (Nota preliminar). *Physis*, **21**, 109–18.

REYES-PUIG, J. P., REYES-PUIG, C., RON, S., ORTEGA, J. A., GUAYASAMIN, J. M., GOODRUM, M., RECALDE, F., VIEIRA, J. J., KOCH, C. and YÁNEZ-MUÑOZ, M. H. 2019. A new species of terrestrial frog of the genus *Noblella* Barbour, 1930 (Amphibia: Strabomantidae) from the Llanganates-Sangay Ecological Corridor, Tungurahua, Ecuador. *PeerJ*, **7**, e7405.

ROČEK, Z., GARDNER, J. D., EATON, J. G. and PŘIKRYL, T. 2013. Anuran ilia from the Upper Cretaceous of Utah-Diversity and stratigraphic patterns. 273–294. *In* TITUS, A. L. and LOWEN, M. A. (eds). *At the Top of the Grand Staircase: The Late Cretaceous of Southern Utah*. Indiana University Press, Bloomington, Indiana, 656 pp.

RODDAZ, M., HERMOZA, W., MORA, A., BABY, P., PARRA, M., CHRISTOPHOUL, F. and ESPURT, N. 2010. Cenozoic sedimentary evolution of the Amazonian foreland basin system. 61–88. *In* HOORN, C. and WESSELINGH, F. P. (eds). *Amazonia, landscape and species evolution: a look into the past*. John Wiley & Sons, Chichester, West Sussex, 464 pp.

ROELANTS, K., GOWER, D. J., WILKINSON, M., LOADER, S. P., BIJU, S. D., GUILLAUME, K., MORIAU, L. and BOSSUYT, F. 2007. Global patterns of diversification in the history of modern amphibians. *Proceedings of the National Academy of Sciences of the United States of America*, **104**, 887–892.

STARRETT, P. H. 1973. Evolutionary patterns in larval morphology. 253–271. In VIAL, J. L. (ed.) *Evolutionary biology of the anurans: Contemporary research on major problems*. University of Missouri Press.

STUART, S. N., CHANSON, J. S., COX, N. A., YOUNG, B. E., RODRIGUES, A. S. L., FISCHMAN, D. L. and WALLER, R. W. 2004. Status and trends of amphibian declines and extinctions worldwide. *Science*, **306**, 1783–1786.

STUTZ, N. S., ABELLO, M. A., MARIVAUX, L., BOIVIN, M., PUJOS, F., BENITES-PALOMINO, A. M., SALAS-GISMONDI, R., TEJADA-LARA, J. V., ANDRIOLLI CUSTÓDIO, M., RODDAZ, M., VENTURA SANTOS, R., RIBEIRO, A. R. and ANTOINE, P.-O. 2022. Late middle Miocene Metatheria (Mammalia) from Juan Guerra, San Martín Department, Peruvian Amazonia. *Journal of South American Earth Sciences*, **118**, 103902.

SUAZO LARA, F. and GÓMEZ, R. O. 2022. In the shadow of dinosaurs: Late Cretaceous frogs are distinct components of a widespread tetrapod assemblage across Argentinean and Chilean Patagonia. *Cretaceous Research*, **131**, 105085.

TOUMOULIN, A., DONNADIEU, Y., LADANT, J. B., BATENBURG, S. J., POBLETE, F. and DUPONT-NIVET, G. 2020. Quantifying the effect of the Drake Passage opening on the Eocene Ocean. *Paleoceanography & Paleoclimatology*, **35** (8), e2020PA003889.

TURAZZINI, G. F. and GÓMEZ, R. O. 2023*a*. A new old Budgett frog: anarticulated skeleton of an Early Pliocene *Lepidobatrachus* (Anura, Ceratophryidae) from western Argentina. *Journal of Vertebrate Paleontology*, **42**, e2207092.

TURAZZINI, G. F. and GÓMEZ, R. O. 2023*b*. Comparative osteology of paradoxical frogs (Hylidae: Pseudae) with comments on diagnostic features, evolutionary trends and potential aquatic adaptations. *Zoologischer Anzeiger*, **43**, 47–70.

TURAZZINI, G. F., TAGLIORETTI, M. L. and GÓMEZ, R. O. 2016. First fossil record of the South American frog genus *Odontophrynus* Reinhardt and Lütken, 1862 (Anura, Neobatrachia). *Journal of Vertebrate Paleontology*, **36**, e1228657.

VACHER, J. P., CHAVE, J., FICETOLA, F. G., SOMMERIA-KLEIN, G., TAO, S., THÉBAUD, C., BLANC, M., CAMACHO, A., CASSIMIRO, J., COLSTON, T. J., DEWYNTER, M., ERNST, R., GAUCHER, P., GOMES, J. O., JAIRAM, R., KOK, P. J. R., LIMA, J. D., MARTINEZ, Q., MARTY, C., NOONAN, B. P., NUNES, P. M. S., OUBOTER, P., RECODER, R., RODRIGUES, M. T., SNYDER, A., MARQUES-SOUZA, S. and FOUQUET, A. 2020. Large-scale DNA-based survey of frogs in Amazonia suggests a vast underestimation of species richness and endemism. *Journal of Biogeography*, **47**, 1781–1791.

VASCONCELOS, T. S., DA SILVA, F. R., DOS SANTOS, T. G., PRADO, V. H. M. and PROVETE, D. B. 2019. South American Anurans: Species Diversity and Description Trends Through Time and Space. 9–84. *In* VASCONCELOS, T. S., DA SILVA, F. R., DOS SANTOS, T. G., PRADO, V. H. M. and PROVETE, D. B. (eds). *Biogeographic Patterns of South American Anurans*. Springer International Publishing New York, 149 pp.

WESTERHOLD, T., MARWAN, N., DRURY, A. J., LIEBRAND, D., AGNINI, C., ANAGNOSTOU, E., BARNET, J. S., BOHATY, S. M., DE VLEESCHOUWER, D., FLORINDO, F. and FREDERICHS, T. 2020. An astronomically dated record of Earth's climate and its predictability over the last 66 million years. *Science*, **369**, 1383–1387.

WIENS, J. J., SUKUMARAN, J., PYRON, R. A. and BROWN, R. M. 2009. Evolutionary and biogeographic origins of high tropical diversity in old world frogs (Ranidae). *Evolution*, **63**, 1217–1231.

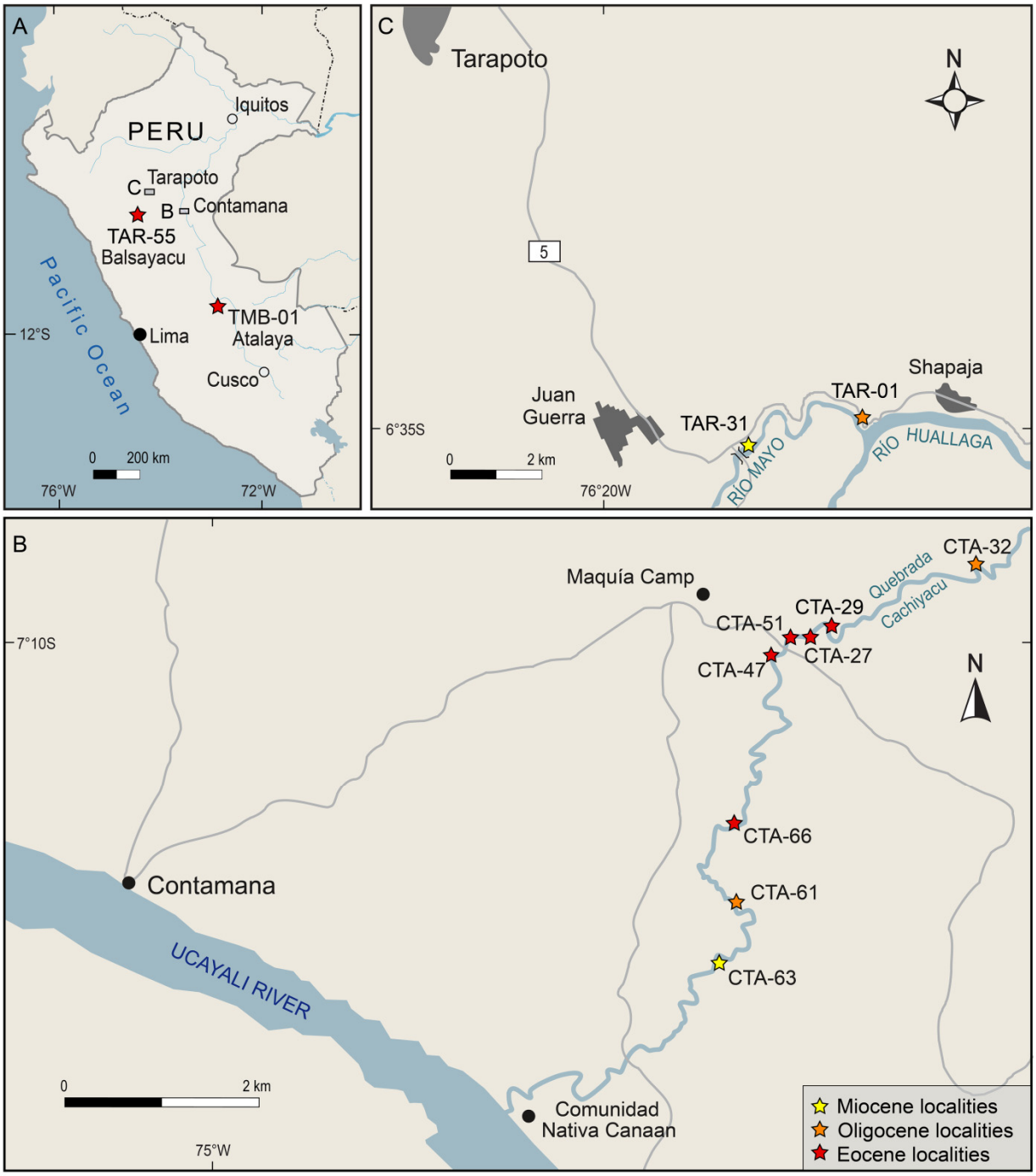

FIG. 1. Location map of the 12 anuran fossil-bearing localities in Peruvian Amazonia. A, map of Peru showing the localities TMB-01 (Río Tambo, Atalaya, Ucayali Basin, Ucayali Department) and TAR-55 (Balsayacu, Huallaga Basin, San Martin Department), and the areas of Contamana (B) and Tarapoto (C). B, map of Contamana area with localities CTA-XX (Ucayali Basin, Loreto Department). C, map of Tarapoto area with localities TAR-01 and TAR-31 (Huallaga Basin, San Martin Department). Maps modified from Antoine *et al*. (2016), Marivaux *et al*. (2020) and Boivin *et al*. (2022).

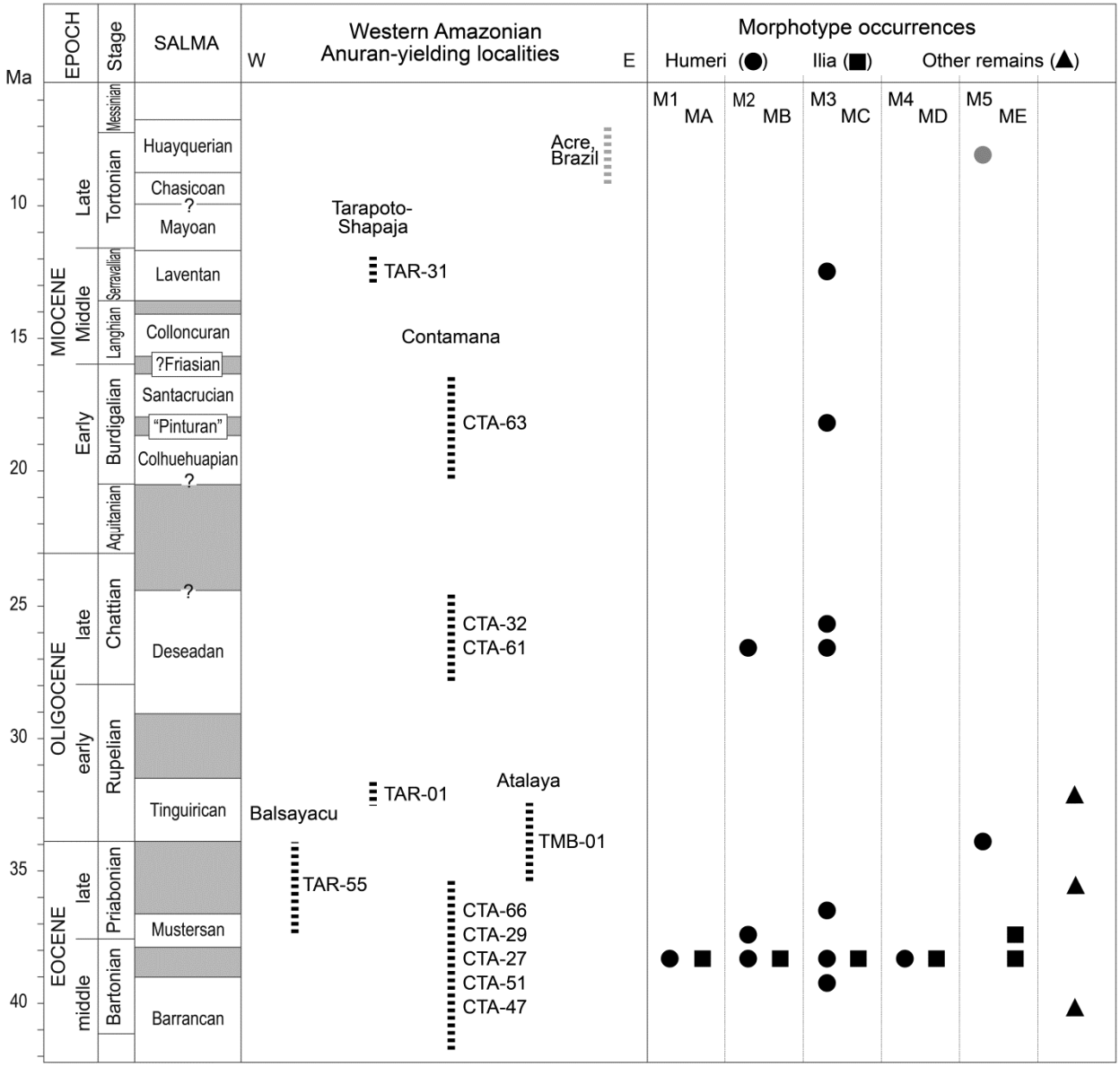

FIG. 2. Fossil anuran-yielding localities and morphotype distribution over time and space in Western Amazonia. Localities originate from the sections of Contamana (CTA-XX), Balsayacu and Shapaja (TAR-YY), and Río Tambo (near Atalaya: TMB-01). Humeral morphotype occurrences are shown with full circles (M1–5) and ilial morphotypes are denoted by black squares (MA–E), whereas triangles point to other remains (not detailed here). Note that no correspondence is hypothesised between humeral and ilial morphotypes in the same column. The previous anuran record (Late Miocene, Brazil; Muniz *et al.* 2022) is indicated in grey. This chart is modified after Halvorsen (2010) and the 2022 International Chronostratigraphic Chart (Cohen *et al*. 2013; updated), Assemat *et al*. (2019), Antoine *et al.* (2021), and Boivin *et al.* (2021) for Peruvian localities. Stratigraphical ages of most localities are tentative (see Antoine *et al*. 2017, 2021; Stutz *et al.* 2022). *Abbreviations*: SALMA, South American Land Mammal Age.

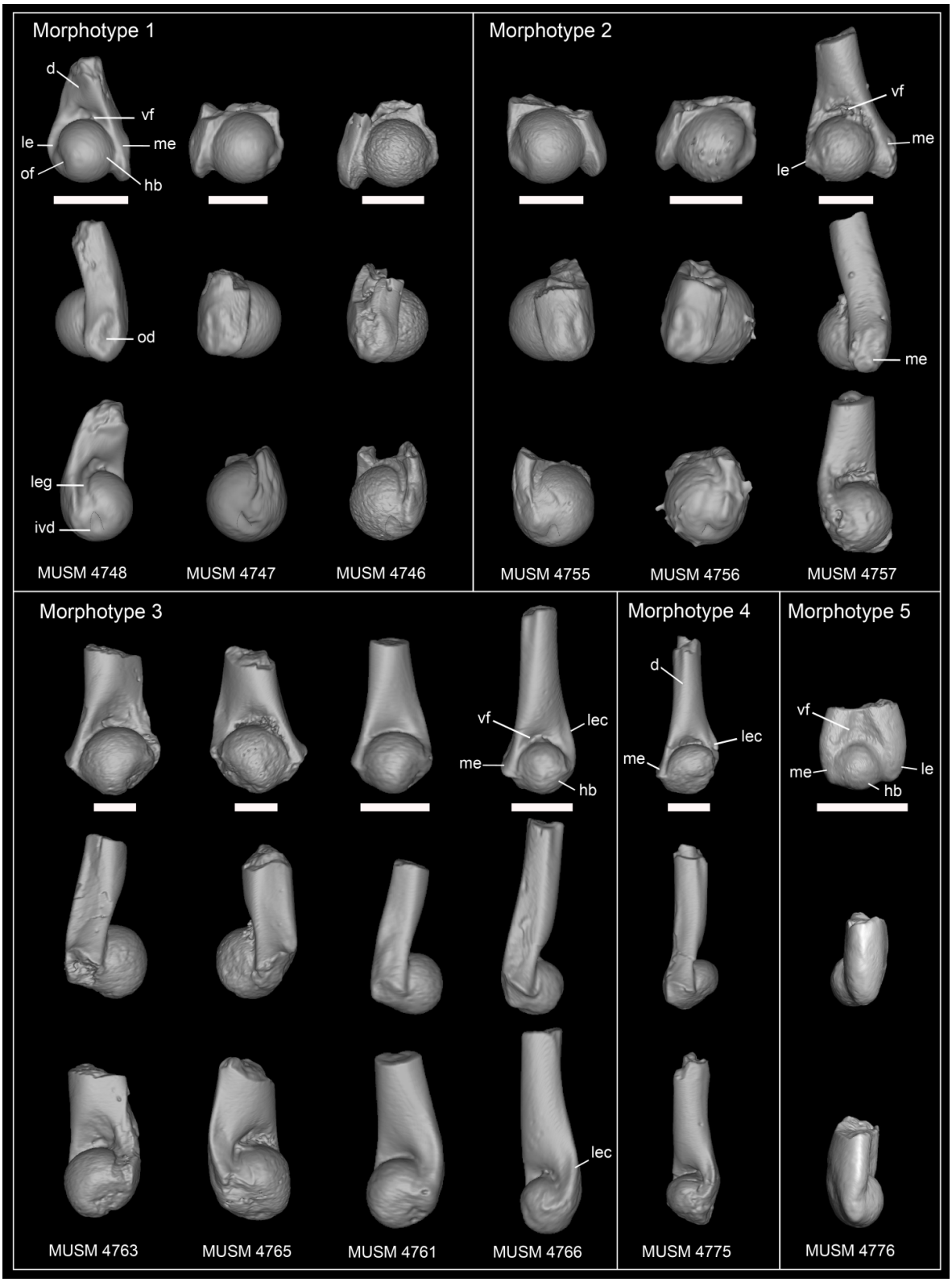

FIG. 3. Humeral morphotypes of Eocene–Miocene anurans from Peruvian Amazonia. From top to bottom: ventral, medial and lateral views. MUSM 4748, MUSM 4755, MUSM 4757, MUSM 4765 and MUSM 4776 correspond to right humeral fragments, whereas the others are left humeral fragments. *Abbreviations*: d, diaphysis; hb, humeral ball; ivd, inverted v-shaped depression; le, lateral epicondyle; lec, lateral epicondylar crest; leg, lateral epicondylar groove; me, medial epicondyle; of, oblique fold; od, oval depression; vf, ventral fossa. The dashed lines delineate the inverted-shaped depression. Scale bars represent 1 mm.

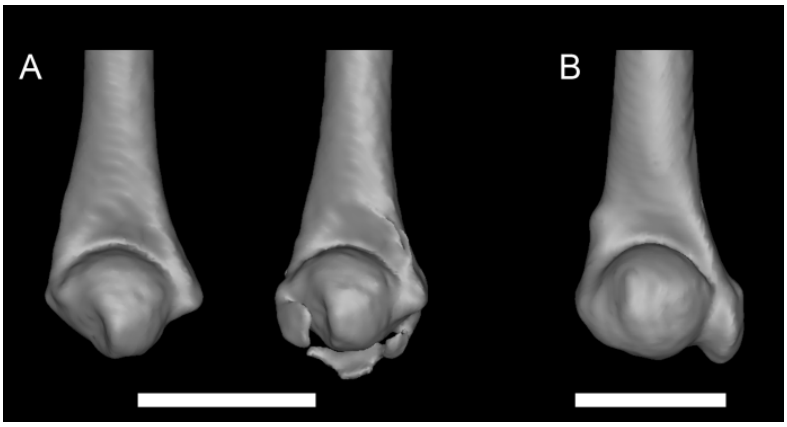

FIG. 4. Ossification variation in distal humeri (in ventral view) of the recent craugastorid frog *Barycholos pulcher*. A, *s*pecimen UF:herp:68063 without (left) and with (right) bone fragments digitally reconstructed in the surroundings of the humeral ball and epicondyles. B, specimen UF:herp:68066. See Table S1 for specimen details. Scale bars represent 1 mm.

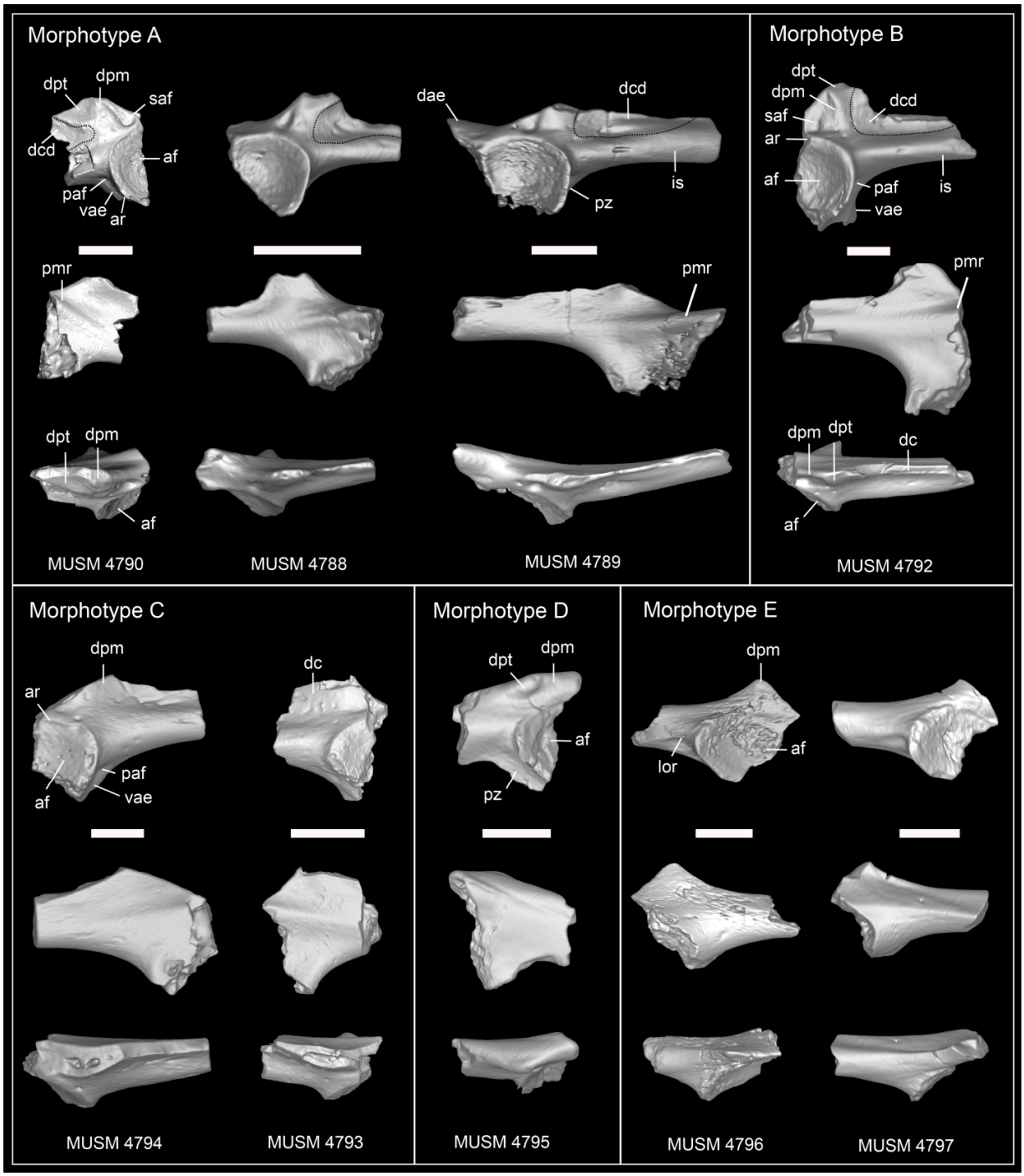

FIG. 5. Anatomical plate of ilial morphotypes of Eocene–Miocene anurans from Peruvian Amazonia. From top to bottom: lateral, medial, and dorsal views. MUSM 4790, MUSM 4793, MUSM 4795, MUSM 4796, and MUSM 4797 correspond to left ilium fragments, while the others are right ilium fragments. *Abbreviations*: af, acetabular fossa; ar, acetabular rim; dae, dorsal acetabular expansion; dc, dorsal crest; dcd, dorsal crest depression; dpm, dorsal prominence; dpt, dorsal protuberance; is, ilial shaft; lor, lateral oblique ridge; paf, pre-acetabular fossa; pmr, proximal medial ridge; pz, pre-acetabular zone (of the ventral acetabular expansion); sf, supra-acetabular fossa. The dashed lines delineate the dorsal crest depression. Scale bars represent 1 mm.

Table 1. Location of anuran fossil-bearing localities in Peruvian Amazonia.

Locality	Lat.(S)	Long.(W)	Formation, member	Hypothesized age	Depositional environment	References
CTA-27	7.33011	74.94733	Pozo, lower member	Late middle Eocene	Fluvial setting	Antoine *et al.* (2016)
CTA-29	7.32859	74.94556	Pozo, lower member	Late middle Eocene	Fluvial setting	Antoine *et al.* (2016)
CTA-32	7.32374	74.93284	Chambira, base	Late Oligocene	Oxbow lake	Antoine *et al.* (2016)
CTA-47	7.33113	74.95127	Pozo, lower member	Middle Eocene	Fluvial setting marine influence	Antoine *et al.* (2016)
CTA-51	7.32948	74.9492	Pozo, lower member	Late middle Eocene	Fluvial setting	Antoine *et al.* (2016)
CTA-61	7.35448	74.95366	Chambira, base	Late Oligocene	Fluvial setting	Antoine *et al.* (2016)
CTA-63	7.36053	74.95551	Pebas, base	Early Miocene (Colhuehuapian)	Lacustrine setting, marine influence	Antoine *et al.* (2016)
CTA-66	7.34876	74.95431	Pozo, lower member	Late middle Eocene	Fluvial setting	Antoine *et al.* (2016)
TAR-01	6.81889	76.51472	Pozo, upper member	Early Oligocene	Marine/littoral setting	Antoine *et al.* (2021)
TAR-31	6.65583	76.39639	Ipururo, lower member	Late middle Miocene	Fluvial setting	Marivaux *et al.* (2020)
TAR-55	7.641389	76.87333	Pozo, lower member	Late middle Eocene	Fluvial, Fluvio-deltaic setting	Boivin *et al.* (2022)
TMB-01	10.88556	73.78972	Pozo, upper member	Latest Eocene-earliest Oligocene	Fluvio-littoral setting	Undescribed

CTA: Contamana (Loreto), TAR: Tarapoto (Juan Guerra-Shapaja-Balsayacu, San Martín), TMB: Río Tambo (Atalaya, Ucayali).

First Eocene-Miocene anuran fossils from Peruvian Amazonia: insights into Neotropical frog evolution and diversity

by OLIVIER JANSEN[1]*, RAÚL ORENCIO GÓMEZ[2]*, ANTOINE FOUQUET[3], LAURENT MARIVAUX[4], RODOLFO SALAS-GISMONDI[5] *and* PIERRE-OLIVIER ANTOINE[4]

[1] Laboratoire Paléontologie Évolution Paléoécosystèmes Paléoprimatologie, Université de Poitiers, UMR CNRS 7262, F-86073 Poitiers, France; olivier.jansen@univ-poitiers.fr; 0009-0003-8770-4915

[2] CONICET-Departamento de Biodiversidad y Biología Experimental, Facultad de Ciencias Exactas y Naturales, Universidad de Buenos Aires, Ciudad Universitaria, C1428EGA Buenos Aires, Argentina; raulorenciogomez@gmail.com; 0000-0002-6600-3787

[3] Laboratoire Évolution et Diversité Biologique, CNRS, F-31062 Toulouse, France; 0000-0003-4060-0281

[4] Laboratoire de Paléontologie, Institut des Sciences de l'Évolution de Montpellier, cc64, Université de Montpellier, CNRS, IRD, F-34095 Montpellier, France; 0000-0002-2882-0874 (Laurent Marivaux); 0000-0001-9122-1818 (Pierre-Olivier Antoine)

[5] Departamento de Paleontología de Vertebrados, Museo de Historia Natural–Universidad Nacional Mayor San Marcos, Avenida Arenales 1256, Lima 11, Peru; 0000-0001-9990-8841

*Corresponding authors

SUPPORTING INFORMATION

Table S1. List of South American species used for the comparison with the Peruvian fossils

The specimens used for the morphological comparisons are illustrated in this table. Species with an (*) correspond to species for which character states were coded. The collection numbers and CT- scanning configurations (resolution, voltage, amperage, and watts) follow MorphoSource indications as stated in https://www.morphosource.org/docs/citation. The column "Resolution (mm)" either corresponds to the CT-scan resolution when a single number is stated and to the bounding box dimensions of the skeleton mesh when three numbers are indicated.

Table S2. Character matrix

The character matrix used for the comparative analysis. Species with numbers at the bottom of the matrix correspond to fossil specimens from Peruvian Amazonia (H: Humeral morphotype, I: ilial morphotype). The single and double asterisks correspond to the specimens uf:herp:68063 and uf:herp:68066, respectively. The description of the characters and their different states follows this matrix.

Table S3. Fossil CT-scan information

The values of voltage (kv), amperage (µa), and watts (W) are provided for each humeral and ilial fossil specimen figured (Figs 3,5). The 3D models of those specimens are available to download on MorphoMuseuM.

Figure S1. Humeri of extant Neotropical anurans

The humerus morphology of extant South American species is illustrated in this figure. The speciesillustrated correspond to species used in the comparative analysis.

Figure S2. Ilia of extant Neotropical anurans

The ilial morphology of extant South American species is illustrated in this figure. The species illustrated correspond to species used in the comparative analysis.

Figure S3. New characters

New characters considered in this study are illustrated in this figure. Each character state is exemplified by an extant Neotropical species used in the comparative analysis.

Table S1: List of South American species used for the comparison with the Peruvian fossils

Family	Species	Material	Specimen	Collection numbers	Unique media identifiers	Resolution/Bounding box (mm)	voltage (kv)	amperage (µa)	watts (W)
Allophrynidae	*Allophryne ruthveni*	Skeleton mesh	000S10946	ku:kuh:166716	doi:10.17602/M2/M26338	6.142, 22.330, 25.511	70	200	0.014
Alsodidae	*Alsodes nodosus*	Skeleton mesh	000S10948	cm:herps:68395	doi:10.17602/M2/M20871	44.349, 12.870, 52.462	130	300	N/A
Alsodidae	*Eupsophus roseus*	Skeleton mesh	000S10954	cm:herps:63926	doi:10.17602/M2/M21082	41.502, 18.439, 68.134	120	300	N/A
Aromobatidae	*Allobates kingsburyi*	Skeleton CT	000S10949	cas:sua:10670	doi:10.17602/M2/M24019	0.019605	100	200	0.02
Aromobatidae	*Aromobates mayorgai*	Skeleton mesh	0000S8695	ku:kuh:132932	ark:/87602/m4/M162124	7.717, 21.557, 42.020	80	200	0.016
Batrachylidae	*Batrachyla taeniata*	Skeleton mesh	000S10959	cas:herp:85253	doi:10.17602/M2/M21960	34.249, 12.356, 41.563	80	150	N/A
Brachycephalidae	*Brachycephalus ephippium**	Skeleton CT	0000S3735	uf:herp:72725	doi:10.17602/M2/M12432	0.012117	100	200	N/A
Brachycephalidae	*Ischnocnema gualteri**	Skeleton CT	0000S3735	uf:herp:72725	doi:10.17602/M2/M12432	0.012117	100	200	N/A
Bufonidae	*Amazophrynella bokermanni*	Skeleton CT	000162004	usnm:amphibians & reptiles:340079	ark:/87602/m4/M162004	18.802, 7.832, 24.826	70	200	0.014
Bufonidae	*Atelopus ignescens*	Skeleton CT	0000S3521	uf:herp:39140	doi:10.17602/M2/M16083	0.025934	100	200	N/A
Bufonidae	*Bufo gargarizans*	Skeleton mesh	000S10638	usnm:amphibians & reptiles:248419	ark:/87602/m4/M160416	60.259, 99.559, 140.783	120	200	0.024
Bufonidae	*Bufotes latastii*	Skeleton mesh	000S12446	uf:herp:81385	ark:/87602/m4/M160418	50.164, 31.639, 98.377	70	200	0.014
Bufonidae	*Epidalea calamita*	Skeleton mesh	000S12562	mvz:amphibian and reptile specimens:mvz:herp:148877	ark:/87602/m4/M162951	50.536, 23.968, 94.109	70	200	0.018
Bufonidae	*Rhinella marina*	Humerus mesh	000S12208	uf:herp:172560	ark:/87602/m4/379385	25.668, 10.646, 14.104	100	200	0.02
Bufonidae	*Rhinella marina*	Skeleton mesh	000S12208	uf:herp:172560	ark:/87602/m4/M163250	83.579, 46.970, 106.845	100	200	0.02
Bufonidae	*Rhinella beebei*	Skeleton mesh	000S27637	RBINS-Scientific Heritage:urn:catalog:RBINS:amp:17147	ark:/87602/m4/M98145	0.039999	100	0.15	N/A
Bufonidae	*Melanophryniscus moreirae*	Skeleton mesh	000S27633	usnm:amphibians & reptiles:207760	ark:/87602/m4/M98144	0.02	100	0.15	N/A
Bufonidae	*Nannophryne variegata*	Skeleton mesh	000S27635	RBINS-Scientific Heritage:urn:catalog:RBINS:amp:12826	ark:/87602/m4/M98210	0.031	100	0.15	N/A
Calyptocephalellidae	*Telmatobufo bullocki (as venustus)*	Skeleton CT	000042671	ku:kuh:161438	doi:10.17602/M2/M42671	0.047731	70	200	0.014
Centrolenidae	*Centrolene buckleyi*	Skeleton mesh	0000S4445	uf:herp:30578	ark:/87602/m4/M16296	25.683, 9.516,68.383	80	220	0.018
Ceratophryidae	*Ceratophrys aurita*	Skeleton mesh	000S10971	cas:herp:84998	ark:/87602/m4/M16100	100.939, 55.627, 126.109	120	200	0.024
Ceratophryidae	*Lepidobatrachus laevis*	Skeleton mesh	0000S4890	uf:herp:12347	ark:/87602/m4/M20355	60.628, 36.209, 135.965	120	150	0.018
Ceratophryidae	*Chacophrys pierottii*	Skeleton mesh	0000S9466	ku:kuh:191932	doi:10.17602/M2/M37697	23.940, 27.055, 35.316	80	200	0.016
Ceuthomantidae	*Ceuthomantis smaragdinus**	Skeleton CT	000S10972	ku:kuh:315000	doi:10.17602/M2/M24438	0.015287	80	190	N/A
Craugastoridae	*Haddadus binotatus**	Skeleton CT	000S11365	usnm:amphibians & reptiles:303295	doi:10.17602/M2/M45297	0.027212	80	200	0.016
Craugastoridae	*Craugastor laticeps*	Skeleton CT	0000S3824	uf:herp:157233	doi:10.17602/M2/M24583	0.043385	100	200	N/A
Craugastoridae	*Craugastor escoces**	Skeleton CT	000S17466	lacm:herps:170147	ark:/87602/m4/M61995	0.060003	100	200	0.02
Craugastoridae	*Tachiramantis prolixodiscus**	Skeleton CT	000S12246	ku:kuh:132728	ark:/87602/m4/M50248	0.025676	80	200	0.016
Cycloramphidae	*Cycloramphus asper*	Skeleton mesh	000S10977	cm:herps:68338	ark:/87602/m4/M22882	56.387, 30.468, 78.140	130	220	0.029

Table S1: List of South American species used for the comparison with the Peruvian fossils

Family	Species	Material	Specimen	Collection numbers	Unique media identifiers	Resolution/Bounding box (mm)	voltage (kv)	amperage (µa)	watts (W)
Dendrobatidae	*Ameerega trivittata**	Skeleton CT	0000S8366	uf:herp:107200	doi:10.17602/M2/M48873	0.033928	100	200	0.02
Dendrobatidae	*Andinobates minutus*	Skeleton CT	000S12914	ypm:vz:ypm hera 020175	ark:/87602/m4/M50176	0.013867	60	200	0.012
Dendrobatidae	*Colostethus inguinalis*	Skeleton CT	000S36504	uf:herp:106871	doi:10.17602/M2/M140395	0.024258	80	200	0.016
Dendrobatidae	*Dendrobates tinctorius**	Skeleton CT	000378710	USNM:Amphibians & Reptiles:247777	ark:/87602/m4/378713	N/A	N/A	N/A	N/A
Dendrobatidae	*Hyloxalus fuliginosus*	Skeleton mesh	000S14774	ku:kuh:182106	ark:/87602/m4/M165116	28.718, 39.765, 33.813	80	160	0.013
Dendrobatidae	*Phyllobates bicolor*	Skeleton CT	0000S8364	uf:herp:71742	doi:10.17602/M2/M28393	0.033053	100	200	0.02
Eleutherodactylidae	*Eleutherodactylus atkinsi**	Skeleton CT	0000S5599	uf:herp:177996	doi:10.17602/M2/M24663	0.028854	80	160	0.013
Eleutherodactylidae	*Eleutherodactylus cuneatus**	Humerus mesh	000S17517	usnm:amphibians & reptiles:5202	ark:/87602/m4/421787	3.339, 3.516, 9.719	80	200	0.016
Eleutherodactylidae	*Eleutherodactylus glaphycompus*	Skeleton mesh	0000S4471	uf:herp:56811	ark:/87602/m4/421787	29.028, 8.415, 44.118	100	200	N/A
Eleutherodactylidae	*Eleutherodactylus karlschmidti**	Skeleton CT	0000S4479	uf:herp:24198	doi:10.17602/M2/M99985	0.041152	120	200	N/A
Eleutherodactylidae	*Eleutherodactylus pipilans*	Skeleton CT	000S15609	uf:herp:104284	doi:10.17602/M2/M58451	0.026772	80	200	0.016
Eleutherodactylidae	*Eleutherodactylus richmondi**	Skeleton CT	000S17496	uf:herp:100531	doi:10.17602/M2/M62041	0.037853	70	200	0.014
Eleutherodactylidae	*Eleutherodactylus ricordii*	Skeleton CT	000S12391	uf:herp:179253	ark:/87602/m4/M48914	0.020321	70	200	0.014
Eleutherodactylidae	*Eleutherodactylus sp.*	Ilium mesh	000S21904	uf:uf/fgs:6086	ark:/87602/m4/M72290	1.065, 3.116, 0.654	85	60	0.005
Eleutherodactylidae	*Diasporus diastema**	Skeleton CT	000S12434	uf:herp:156143	doi:10.17602/M2/M49075	0.024092	70	200	0.014
Eleutherodactylidae	*Phyzelaphryne miriamae**	Skeleton CT	0000S8003	usnm:amphibians & reptiles:239363	doi:10.17602/M2/M33058	0.009775	70	300	N/A
Eleutherodactylidae	*Adelophryne gutturosa**	Skeleton CT	000S10265	usnm:amphibians & reptiles:549315	doi:10.17602/M2/M40365	0.021926	70	300	N/A
Hemiphractidae	*Gastrotheca peruana*	Skeleton CT	0000S4441	uf:herp:65801	doi:10.17602/M2/M55543	0.043445	100	200	N/A
Hylidae	*Acris gryllus*	Skeleton mesh	0000S4822	uf:herp:107362	doi:10.17602/M2/M20037	24.534, 26.955, 5.112	100	200	N/A
Hylidae	*Aplastodiscus perviridis*	Skeleton mesh	000S10437	ku:kuh:92722	ark:/87602/m4/M160405	17.807, 35.712, 39.086	80	200	0.016
Hylidae	*Dendropsophus marmoratus*	Skeleton CT	000S34788	uf:herp:43240	ark:/87602/m4/M133973	0.023601	60	200	0.012
Hylidae	*Hyla cinerea*	Skeleton CT	0000S4882	uf:herp:123473	ark:/87602/m4/M20332	0.031721	100	150	N/A
Hylidae	*Hyla goini*	Ilium mesh	000S21907	uf:uf/fgs:11426	ark:/87602/m4/M72296	6.268, 5.922, 2.369	85	60	0.005
Hylidae	*Osteocephalus taurinus**	Skeleton CT	000S28509	uf:herp:27081	doi:10.17602/M2/M101196	0.054896	80	200	0.016
Hylidae	*Scinax staufferi*	Skeleton CT	000S12528	uf:herp:137479	ark:/87602/m4/M49250	0.021601	90	150	0.013
Hylidae	*Xenohyla truncata*	Skeleton mesh	000S28467	ku:kuh:92190	ark:/87602/m4/M165523	27.022, 11.605, 38.505	70	200	0.014
Hylodidae	*Crossodactylus trachystomus*	Skeleton mesh	000S10976	cm:herps:2662	ark:/87602/m4/M24014	18.231, 9.207, 47.328	130	220	0.023

Table S1: List of South American species used for the comparison with the Peruvian fossils

Family	Species	Material	Specimen	Collection numbers	Unique media identifiers	Resolution/Bounding box (mm)	Voltage (kv)	Amperage (µa)	Watts (W)
Hylodidae	*Megaelosia goeldii*	Skeleton mesh	000423172	USNM:Amphibians & Reptiles:208564	ark:/87602/m4/423209	855.300, 503.201, 1071.980	N/A	N/A	N/A
Leptodactylidae	*Adenomera andreae**	Skeleton CT	0000S4067	uf:herp:43260	doi:10.17602/M2/M114556	0.026539	100	200	N/A
Leptodactylidae	*Crossodactylodes sp.*	Skeleton CT	000S12821	cas:sua:11774	ark:/87602/m4/M46051	0.028849	125	150	0.019
Leptodactylidae	*Edalorhina perezi**	Skeleton CT	000S12818	cas:sua:11446	ark:/87602/m4/M49876	0.025785	70	140	0.014
Leptodactylidae	*Engystomops pustulosus*	Skeleton CT	000S12819	cas:sua:21892	ark:/87602/m4/M49917	0.024850	80	190	0.015
Leptodactylidae	*Hydrolaetare schmidti*	Skeleton CT	000S12215	ku:kuh:220904	ark:/87602/m4/M48509	0.068028	110	200	0.002
Leptodactylidae	*Leptodactylus albilabris*	Skeleton CT	000S17498	uf:herp:37017	doi:10.17602/M2/M62049	0.045508	70	200	0.014
Leptodactylidae	*Leptodacylus pentadactylus*	Skeleton CT	000S12828	uf:herp:103788	ark:/87602/m4/M50004	0.075450	100	200	0.02
Leptodactylidae	*Leptodactylus poecilochilus*	Skeleton CT	000S12547	uf:herp:103913	ark:/87602/m4/M49383	0.062904	100	200	0.02
Leptodactylidae	*Leptodactylus validus**	Skeleton CT	000S12548	uf:herp:103921	ark:/87602/m4/M49384	0.039500	100	200	0.02
Leptodactylidae	*Pleurodema nebulosum**	Skeleton CT	000S12820	cas:sua:15635	ark:/87602/m4/M46050	0.022870	125	150	0.019
Leptodactylidae	*Pleurodema nebulosum**	Humerus mesh	000S12820	cas:sua:15635	ark:/87602/m4/379379	0.022870	125	150	0.019
Leptodactylidae	*Pseudopaludicola falcipes*	Skeleton CT	000S12924	ypm:vz:ypm hera 009648	ark:/87602/m4/M50161	0.017834	60	200	0.012
Leptodactylidae	*Paratelmatobius lutzii*	Skeleton CT	000S17518	usnm:amphibians & reptiles:525811	ark:/87602/m4/M62082	0.027853	70	200	0.014
Leptodactylidae	*Scythrophrys sawayae*	Skeleton CT	000364517	USNM:Amphibians & Reptiles:137662	ark:/87602/m4/364520	0.013011	80	150	0.012
Microhylidae	*Chiasmocleis royi*	Skeleton CT	0000S5020	usnm:amphibians & reptiles:269001	ark:/87602/m4/M50046	0.021506	80	180	0.014
Microhylidae	*Ctenophryne geayi*	Skeleton CT	000364549	AMNH:Herpetology:A-166441	ark:/87602/m4/364552	0.034064	70	300	0.021
Microhylidae	*Hamptophryne boliviana*	Skeleton CT	000S41368	amnh:herpetology:a-115764	ark:/87602/m4/M154612	0.040019	70	300	0.021
Microhylidae	*Gastrophryne carolinensis*	Ilium mesh	000S21888	uf:uf:5144	ark:/87602/m4/M72243	4.962, 2.396, 1.272	85	60	0.005
Odontophrynidae	*Odontophrynus americanus*	Skeleton mesh	0000S5541	cm:herps:147828	doi:10.17602/M2/M25346	50.644, 25.253, 67.276	130	220	0.029
Phyllomedusidae	*Agalychnis callidryas*	Skeleton mesh	000S12834	cas:herp:146957	ark:/87602/m4/M161987	40.150, 22.322, 51.741	80	200	0.016
Phyllomedusidae	*Phyllomedusa hypochondrialis*	Skeleton CT	000S45193	amnh:herpetology:a-166281	ark:/87602/m4/M165653	0.029426	80	200	0.016
Pipidae	*Pipa aspera**	Skeleton CT	000S45338	mvz:amphibian and reptile specimens:mvz:herp:247507	ark:/87602/m4/M165891	0.027501	80	200	0.016
Pipidae	*Pipa parva**	Skeleton CT	0000S3720	uf:herp:37924	doi:10.17602/M2/M12424	0.022456	120	160	N/A
Pipidae	*Pipa carvalhoi**	Skeleton CT	162105	mcz:herp:a-25737	ark:/87602/m4/M162105	0,02486	50	150	0,0075
Pipidae	*Pipa carvalhoi**	Dry skeleton	-	MACN-HE 42608	-	N/A	N/A	N/A	N/A
Pipidae	*Pipa pipa**	Skeleton CT	000405740	USNM:Amphibians & Reptiles:85032	ark:/87602/m4/405740	0.119553	N/A	N/A	N/A
Pipidae	*Pipa pipa**	Dry skeleton	-	MACN-HE 42612	-	N/A	N/A	N/A	N/A

Table S1: List of South American species used for the comparison with the Peruvian fossils

Family	Species	Material	Specimen	Collection numbers	Unique media identifiers	Resolution/Bounding box (mm)	Voltage (kv)	Amperage (µa)	Watts (W)
Pipidae	*Pipa snethlageae**	Dry skeleton	-	MACN-HE 42611	-	N/A	N/A	N/A	N/A
Pipidae	*Pipa snethlageae**	Skeleton CT	000066254	mcz:herp:a-17734	ark:/87602/m4/M66254	0.029011	50	150	0.0075
Rhinodermatidae	*Rhinoderma darwinii*	Skeleton mesh	0000S5575	uf:herp:62022	doi:10.17602/M2/M25059	18.025, 13.445, 48.031	100	150	0.15
Strabomantidae	*Barycholos pulcher-1**	Skeleton CT	0000S4527	uf:herp:68063	ark:/87602/m4/M22665	0.023678	90	150	N/A
Strabomantidae	*Barycholos pulcher-2**	Skeleton CT	0000S8363	uf:herp:68066	doi:10.17602/M2/M26384	0.026917	100	200	0.02
Strabomantidae	*Bryophryne cophites*	Skeleton CT	000S17453	ku:kuh:173293	ark:/87602/m4/M61982	0.020901	100	200	0.02
Strabomantidae	*Niceforonia araiodactyla**	Skeleton CT	0000S5268	uf:herp:40764	doi:10.17602/M2/M26269	0.017563	100	250	N/A
Strabomantidae	*Noblella myrmecoides**	Skeleton CT	000S14767	mcz:herp:a-89110	ark:/87602/m4/M58632	0.008255	45	175	0.008
Strabomantidae	*Oreobates quixensis**	Skeleton CT	000S11006	cas:sua:11453	doi:10.17602/M2/M24439	0.031084	80	150	0.012
Strabomantidae	*Pristimantis duellmani**	Skeleton CT	000S17455	ku:kuh:179333	ark:/87602/m4/M61984	0.042835	100	200	0.02
Strabomantidae	*Pristimantis galdi*	Skeleton CT	000S25892	fmnh:amphibians and reptiles:28065	ark:/87602/m4/M88066	0.028107	100	200	0.02
Strabomantidae	*Pristimantis vinhai**	Skeleton CT	000S12855	usnm:amphibians & reptiles:284544	doi:10.17602/M2/M50047	0.016197	70	300	0.021
Strabomantidae	*Psychrophrynella bagrecito*	Humerus mesh	000S45588	amnh:herpetology:a-159115	ark:/87602/m4/379388	4.563, 1.500, 1.229	70	200	0.014
Strabomantidae	*Strabomantis anomalus**	Skeleton CT	000S11021	cas:herp:119754	doi:10.17602/M2/M24024	0.036755	100	150	0.015
Strabomantidae	*Strabomantis biporcatus**	Skeleton CT	000S12719	cas:herp:119580	doi:10.17602/M2/M49883	0.019833	100	150	0.015
Strabomantidae	*Strabomantis cornutus*	Skeleton CT	000S12810	cas:sua:11456	doi:10.17602/M2/M49878	0.034841	100	150	0.015
Strabomantidae	*Strabomantis ingeri*	Skeleton CT	000S12880	fmnh:amphibians and reptiles:81915	doi:10.17602/M2/M50228	0.028803	100	120	0.012
Strabomantidae	*Strabomantis sulcatus*	Skeleton CT	000S12811	cas:sua:11451	doi:10.17602/M2/M49877	0.063197	100	150	0.015
Telmatobiidae	*Telmatobius carrillae*	Humerus mesh	000S44360	uf:herp:39717	ark:/87602/m4/379382	12.090, 3.197, 4.824	80	200	0.016
Telmatobiidae	*Telmatobius thompsoni*	Skeleton mesh	0000S4886	uf:herp:39734	doi:10.17602/M2/M20345	65.510, 27.985, 110.355	120	150	0.018

Table S2: character matrix (humeral characters)

Species/specimens	1	2	3	4	5	6	7	8	9	10	11	12	13	14	15	16	17	18	19	20	21	22
Ceuthomantis smaragdinus	0	0	1	1	0	0	1	2	0	0	0	0	1	2	0	0	2	1	1	0	1	1
Eleutherodactylus karlschmidti	0	1	1	1	2	1	1	2	0	1	0	2	0	2	0	0	2	1	1	0	0	1
Eleutherodactylus cuneatus	0	0	1	1	0	0	1	2	0	0	0	1	1	2	0	0	2	1	2	0	1	1
Eleutherodactylus richmondi	1	0	1	0	1	1	0	0	1	0	2	1	1	0	1	0	1	1	2	0	0	1
Eleutherodactylus atkinsi	0	0	1	0	1	1	0	0	1	0	2	1	0	0	1	0	1	1	1	0	0	1
Diasporus diastema	1	0	1	0	0	1	0	0	1	0	1	0	1	0	?	0	0	1	1	0	0	0
Phyzelaphryne miriamae	1	0	1	0	1	?	0	0	1	0	2	1	1	0	1	0	1	1	2	0	0	1
Adelophryne gutturosa	1	1	1	0	1	1	0	0	1	1	2	1	1	0	1	0	1	1	1	0	0	1
Brachycephalus ephippium	2	1	0	0	1	0	0	0	1	1	1	1	0	0	?	0	1	0	0	1	1	1
Ischnocnema gualteri	1	1	1	0	0	0	0	0	1	0	2	0	0	1	1	0	0	0	2	0	0	1
Haddadus binotatus	1	1	1	2	2	0	1	2	0	1	0	1	0	2	0	0	2	0	0	0	1	1
Craugastor escoces	1	1	1	1	0	0	0	0	1	1	2	1	0	0	1	0	0	0	0	0	1	1
Tachiramantis prolixodiscus	2	1	1	0	0	0	0	1	1	2	1	1	1	0	0	0	0	0	0	0	1	0
Oreobates quixensis	?	1	1	0	1	0	0	0	1	1	1	1	1	0	1	0	1	0	0	0	1	1
Strabomantis anomalus	0	1	1	2	0	0	1	2	0	2	0	2	1	2	0	0	2	0	1	0	1	1
Strabomantis biporcatus	0	1	1	2	0	0	1	2	0	2	0	2	1	2	0	0	2	0	1	0	0	1
Pristimantis vinhai	0	0	1	0	0	1	0	0	1	2	1	2	1	1	1	0	0	0	1	0	1	0
Pristimantis duellmani	1	1	0	0	0	0	0	0	1	2	1	2	1	1	0	0	1	0	1	0	1	0
Niceforonia araiodactyla	0	0	1	2	0	0	1	2	0	0	0	0	1	2	0	0	2	0	2	0	0	1
Noblella myrmecoides	0	0	1	0	1	0	0	0	1	0	1	1	1	0	0	1	1	1	2	0	1	0
*Barycholos pulcher**	0	0	1	1	0	0	0	1	0	0	0	1	1	2	0	0	2	1	1	0	0	1
*Barycholos pulcher***	0	0	1	0	1	?	0	1	1	0	2	1	1	0	1	0	1	1	1	0	0	1
Leptodactylus latrans	?	?	?	?	?	?	?	?	?	?	?	?	?	?	?	?	?	?	?	?	?	?
Leptodactylus validus	2	1	1	0	0	?	0	0	1	0	2	2	0	0	1	0	0	1	2	1	1	0
Adenomera andreae	2	0	1	0	0	0	0	0	1	0	2	2	1	0	0	1	0	1	2	0	0	0
Pleurodema nebulosa	1	1	1	0	1	?	0	0	1	0	1	2	0	1	1	1	1	1	2	0	0	0
Edalorhina perezi	0	0	1	0	1	?	0	0	1	0	2	1	1	1	1	0	1	1	0	0	1	1
Dendrobates tinctorius	0	0	1	0	0	0	0	0	1	0	1	1	1	1	1	1	0	1	1	0	0	0
Ameerega trivittata	0	0	1	0	0	0	0	0	1	0	1	1	1	1	1	1	0	0	1	0	0	0
Osteocephalus taurinus	0	1	1	0	0	0	0	0	1	1	1	2	0	1	1	1	0	0	1	1	1	1
Pipa snethlageae	1	0	0	0	0	0	0	1	2	1	2	1	1	2	0	1	0	0	0	0	0	0
Pipa pipa	0	0	0	0	0	0	0	1	2	1	2	1	1	2	0	1	0	0	0	0	0	0
Pipa carvalhoi	1	0	0	0	0	0	0	1	1	1	1	1	1	0	0	1	0	0	0	0	0	0
Pipa parva	1	0	0	0	0	0	0	1	1	1	1	1	1	0	0	1	0	0	0	0	0	0
Pipa aspera	1	0	0	0	0	0	0	1	1	1	1	1	1	0	0	1	0	0	0	0	0	0
MUSM 4746 (H1)	?	?	1	0	0	1	0	0	1	0	2	1	?	0	?	0	1	1	1	?	?	?
MUSM 4747 (H1)	?	?	1	0	1	1	0	0	1	0	2	1	?	0	1	1	1	1	0	?	?	?
MUSM 4748 (H1)	?	?	1	0	1	1	0	0	1	0	2	1	1	0	1	0	1	1	1	0	0	1
MUSM 4755 (H2)	?	?	1	0	1	1	0	0	1	0	1	1	?	0	1	0	1	1	2	?	?	?
MUSM 4756 (H2)	?	?	1	0	1	1	0	0	1	0	1	1	?	0	1	0	1	1	2	?	?	?
MUSM 4757 (H2)	?	?	1	0	1	1	0	0	1	0	2	1	1	0	1	0	1	?	2	0	0	1
MUSM 4761 (H3)	?	?	1	1	0	0	0	1	0	0	0	0	1	2	0	0	2	1	2	0	1	1
MUSM 4763 (H3)	?	?	1	1	0	0	0	1	0	0	0	0	1	2	0	0	2	1	?	0	?	1
MUSM 4765 (H3)	?	?	1	1	0	0	0	1	0	?	0	0	1	2	0	0	2	1	?	0	1	1
MUSM 4766 (H3)	?	?	1	1	0	0	0	1	0	0	0	0	1	2	0	0	2	1	2	0	1	1
MUSM 4775 (H4)	?	?	1	1	0	0	1	2	0	0	0	0	1	2	0	0	?	1	0	0	1	1
MUSM 4776 (H5)	?	?	0	0	0	0	0	1	1	0	1	0	?	0	0	1	0	0	0	0	0	0
MUSM 4788 (IA)	?	?	?	?	?	?	?	?	?	?	?	?	?	?	?	?	?	?	?	?	?	?
MUSM 4789 (IA)	?	?	?	?	?	?	?	?	?	?	?	?	?	?	?	?	?	?	?	?	?	?
MUSM 4790 (IA)	?	?	?	?	?	?	?	?	?	?	?	?	?	?	?	?	?	?	?	?	?	?
MUSM 4792 (IB)	?	?	?	?	?	?	?	?	?	?	?	?	?	?	?	?	?	?	?	?	?	?
MUSM 4793 (IC)	?	?	?	?	?	?	?	?	?	?	?	?	?	?	?	?	?	?	?	?	?	?
MUSM 4794 (IC)	?	?	?	?	?	?	?	?	?	?	?	?	?	?	?	?	?	?	?	?	?	?
MUSM 4795 (ID)	?	?	?	?	?	?	?	?	?	?	?	?	?	?	?	?	?	?	?	?	?	?
MUSM 4796 (IE)	?	?	?	?	?	?	?	?	?	?	?	?	?	?	?	?	?	?	?	?	?	?
MUSM 4797 (IE)	?	?	?	?	?	?	?	?	?	?	?	?	?	?	?	?	?	?	?	?	?	?

Table S2: character matrix (ilial and ischial characters)

Species/specimens	23	24	25	26	27	28	29	30	31	32	33	34	35	36	37	38	39	40	41	42	43	44	45	46	47	48	49	50	51	52	53
Ceuthomantis smaragdinus	0	0	1	1	0	2	1	1	3	1	0	1	1	2	3	0	0	0	2	0	2	1	1	0	1	0	1	0	0	0	1
Eleutherodactylus karlschmidti	1	0	1	1	2	0	1	1	3	1	0	0	2	2	3	0	0	0	0	0	2	1	1	1	1	0	1	0	0	0	1
Eleutherodactylus cuneatus	?	?	?	?	?	?	?	?	?	?	?	?	?	?	?	?	?	?	?	?	?	?	?	?	?	?	?	?	?	?	?
Eleutherodactylus richmondi	1	1	1	1	2	0	2	1	3	2	0	0	2	2	3	0	0	0	0	0	2	1	1	1	1	0	1	0	0	1	2
Eleutherodactylus atkinsi	1	1	1	1	2	0	2	1	1	2	1	0	2	2	3	0	0	0	0	0	2	0	1	1	1	0	1	0	0	1	2
Diasporus diastema	1	1	1	1	2	2	2	1	1	2	0	0	2	2	3	0	0	0	0	0	2	0	1	2	1	0	1	0	0	1	2
Phyzelaphryne miriamae	1	0	0	1	3	2	2	1	3	2	0	0	2	2	3	0	0	0	0	0	2	1	1	1	1	0	3	1	1	1	2
Adelophryne gutturosa	1	1	0	1	3	2	2	1	1	2	0	0	2	2	3	0	0	0	0	0	2	1	1	1	1	0	3	1	1	1	3
Brachycephalus ephippium	2	0	1	1	0	2	2	1	2	2	0	1	2	2	3	1	0	0	2	0	2	1	0	2	1	0	3	1	1	1	0
Ischnocnema gualteri	1	0	1	1	2	0	2	1	3	2	0	0	2	2	3	0	0	0	0	0	2	0	1	2	1	0	3	1	0	0	1
Haddadus binotatus	0	2	1	1	2	2	2	1	3	1	0	0	2	2	3	1	0	0	2	0	2	1	1	0	1	0	1	0	0	0	3
Craugastor escoces	1	0	1	1	2	0	2	1	3	1	0	0	2	2	3	0	0	0	0	0	2	0	1	0	1	0	1	0	1	1	3
Tachiramantis prolixodiscus	1	1	1	0	0	2	1	1	1	1	0	1	1	2	3	0	0	0	2	0	2	0	1	2	0	0	1	0	0	0	3
Oreobates quixensis	0	0	1	1	3	0	2	1	3	1	0	0	2	2	3	0	0	0	1	0	2	1	1	0	1	0	1	0	0	0	2
Strabomantis anomalus	1	1	1	1	3	1	2	1	3	1	0	0	2	2	3	1	0	0	1	0	2	1	1	0	1	0	1	0	?	?	?
Strabomantis biporcatus	1	1	1	1	3	1	2	1	3	1	0	0	2	2	3	1	0	0	2	0	2	1	1	0	1	0	1	0	?	?	?
Pristimantis vinhai	1	1	1	0	3	0	1	1	1	1	0	0	1	2	3	0	0	0	0	0	2	0	1	2	1	0	1	0	0	1	3
Pristimantis duellmani	1	1	1	0	0	2	1	1	1	1	0	0	1	2	3	0	0	0	0	0	2	0	1	2	0	0	1	0	0	1	3
Niceforonia araiodactyla	1	2	1	0	3	2	2	1	0	1	0	0	1	2	3	0	0	0	2	0	2	1	1	0	1	0	1	0	?	?	?
Noblella myrmecoides	4	1	1	1	2	2	2	1	3	1	0	0	2	2	3	0	0	0	0	0	2	0	1	2	0	0	1	1	1	1	3
*Barycholos pulcher**	0	1	1	1	2	2	2	1	3	1	0	0	2	2	0	1	0	0	1	0	2	1	1	0	1	0	1	0	0	1	1
*Barycholos pulcher***	0	1	1	1	2	2	2	1	3	1	0	0	2	2	0	1	0	0	0	0	2	0	1	2	1	0	1	1	0	1	2
Leptodactylus latrans	?	?	?	1	2	?	1	1	3	1	0	0	2	?	?	1	0	?	0	1	0	1	1	1	1	0	1	0	?	?	?
Leptodactylus validus	1	1	1	1	2	0	1	1	3	1	0	0	2	2	3	1	0	0	0	1	0	1	1	1	1	0	1	0	0	1	2
Adenomera andreae	0	1	1	1	2	0	1	1	3	1	0	0	2	2	3	0	0	0	0	1	0	1	1	1	1	0	1	1	1	1	2
Pleurodema nebulosa	0	0	0	2	0	2	1	1	0	1	0	1	1	1	3	0	0	0	2	1	0	1	1	2	0	1	1	0	0	1	1
Edalorhina perezi	3	2	0	1	0	0	1	1	4	1	0	1	1	1	3	0	0	0	2	1	0	1	1	2	0	1	0	0	0	1	1
Dendrobates tinctorius	3	2	1	0	0	2	2	1	0	1	0	0	1	2	3	0	0	0	0	0	0	0	0	1	0	0	1	1	0	0	1
Ameerega trivittata	1	2	1	1	0	2	1	1	0	1	0	0	2	2	3	1	1	0	0	0	0	0	0	1	1	0	1	1	0	0	1
Osteocephalus taurinus	1	2	1	0	3	2	1	1	1	0	0	0	1	1	3	0	0	0	2	0	0	0	0	3	0	0	0	0	0	1	3
Pipa snethlageae	1	2	2	1	0	0	0	1	4	0	0	0	2	0	2	0	1	2	2	2	1	0	0	0	1	1	0	0	0	1	0
Pipa pipa	1	2	2	1	0	0	0	1	4	0	0	0	2	0	2	0	1	2	2	2	1	0	0	0	0	1	0	0	0	1	4
Pipa carvalhoi	1	2	2	1	0	0	0	1	4	0	0	0	2	0	2	0	1	2	2	2	1	0	0	0	0	1	0	0	0	1	4
Pipa parva	1	2	2	1	0	0	0	1	4	0	0	0	2	0	2	0	1	2	2	2	1	0	0	0	0	1	0	0	0	1	4
Pipa aspera	1	2	2	1	0	0	0	1	4	0	0	0	2	0	2	0	1	2	2	2	1	0	0	0	0	1	0	0	0	1	4

Table S2: character matrix (ilial and ischial characters)

Species/specimens	23	24	25	26	27	28	29	30	31	32	33	34	35	36	37	38	39	40	41	42	43	44	45	46	47	48	49	50	51	52	53
MUSM 4746 (H1)	?	?	?	?	?	?	?	?	?	?	?	?	?	?	?	?	?	?	?	?	?	?	?	?	?	?	?	?	?	?	?
MUSM 4747 (H1)	?	?	?	?	?	?	?	?	?	?	?	?	?	?	?	?	?	?	?	?	?	?	?	?	?	?	?	?	?	?	?
MUSM 4748 (H1)	?	?	?	?	?	?	?	?	?	?	?	?	?	?	?	?	?	?	?	?	?	?	?	?	?	?	?	?	?	?	?
MUSM 4755 (H2)	?	?	?	?	?	?	?	?	?	?	?	?	?	?	?	?	?	?	?	?	?	?	?	?	?	?	?	?	?	?	?
MUSM 4756 (H2)	?	?	?	?	?	?	?	?	?	?	?	?	?	?	?	?	?	?	?	?	?	?	?	?	?	?	?	?	?	?	?
MUSM 4757 (H2)	?	?	?	?	?	?	?	?	?	?	?	?	?	?	?	?	?	?	?	?	?	?	?	?	?	?	?	?	?	?	?
MUSM 4761 (H3)	?	?	?	?	?	?	?	?	?	?	?	?	?	?	?	?	?	?	?	?	?	?	?	?	?	?	?	?	?	?	?
MUSM 4763 (H3)	?	?	?	?	?	?	?	?	?	?	?	?	?	?	?	?	?	?	?	?	?	?	?	?	?	?	?	?	?	?	?
MUSM 4765 (H3)	?	?	?	?	?	?	?	?	?	?	?	?	?	?	?	?	?	?	?	?	?	?	?	?	?	?	?	?	?	?	?
MUSM 4766 (H3)	?	?	?	?	?	?	?	?	?	?	?	?	?	?	?	?	?	?	?	?	?	?	?	?	?	?	?	?	?	?	?
MUSM 4775 (H4)	?	?	?	?	?	?	?	?	?	?	?	?	?	?	?	?	?	?	?	?	?	?	?	?	?	?	?	?	?	?	?
MUSM 4776 (H5)	?	?	?	?	?	?	?	?	?	?	?	?	?	?	?	?	?	?	?	?	?	?	?	?	?	?	?	?	?	?	?
MUSM 4788 (IA)	?	?	?	1	1	0	1	1	3	1	0	0	2	?	0	1	0	?	?	?	?	1	1	0	1	0	1	?	?	?	?
MUSM 4789 (IA)	?	?	?	1	?	0	1	?	?	?	0	0	2	?	0	1	0	0	?	0	0	1	1	0	1	0	1	0	?	?	?
MUSM 4790 (IA)	?	?	?	1	1	0	1	1	3	1	0	?	2	?	?	1	0	?	?	?	?	1	1	0	1	0	1	?	?	?	?
MUSM 4792 (IB)	?	?	?	2	1	0	1	1	3	1	0	0	2	?	0	1	0	0	?	?	?	1	1	1	1	0	1	?	?	?	?
MUSM 4793 (IC)	?	?	?	?	?	?	?	?	?	?	?	0	2	?	0	0	0	?	?	?	?	?	?	?	?	0	1	?	?	?	?
MUSM 4794 (IC)	?	?	?	?	?	?	?	?	?	?	?	0	2	?	0	0	0	?	?	?	?	?	?	?	1	0	1	?	?	?	?
MUSM 4795 (ID)	?	?	?	0	0	2	1	1	2	1	0	0	?	?	?	0	0	0	?	?	?	0	0	3	0	0	0	?	?	?	?
MUSM 4796 (IE)	?	?	?	1	0	0	0	0	-	0	0	0	?	?	?	?	1	2	2	2	1	0	1	0	0	0	0	?	?	?	?
MUSM 4797 (IE)	?	?	?	1	?	0	0	0	-	0	0	0	?	?	?	?	1	2	2	2	1	0	1	0	0	0	0	?	?	?	?

Table S2: Character matrix - Character description:

The characters list used in this paper mainly follows that of Báez *et al*. (2012); Gómez & Turazzini (2016, 2021) for the ilial morphology and Blackburn *et al*. (2019, 2020), Gómez & Turazzini (2021), Keeffe & Blackburn (2020) for the humerus morphology. *Abbreviations*: BGT12 (Báez *et al*. 2012); B13 (Báez 2013); G16 (Gómez 2016); GT21 (Gómez & Turazzini 2021). New characters are indicated with (J) and those modified from previous characters are indicated with (J*). New characters and character states are illustrated in Figure S3.

1) Humerus, shaft, general shape: (0) bowed ventrally, but nearly straight or only slightly tilted laterally in ventral view; (1) bowed ventrally and moderately tilted laterally; (2) bowed ventrallyand strongly tilted laterally. (GT21: 236)
2) Humerus, deltoid crest (= crista ventralis), relative length (with respect to the humeral length): (0) short (ratio nearly 1/3); (1) long (ratio nearly 1/2). (G16 :126)
3) Humerus, humeral ball (= eminentia capitata), relative size (as transverse diameter relative to maximum distal width at epicondyle level): (0) small (ratio < 0.58); (1) large (ratio > 0.58). (G16:124)
4) Humerus, humeral ball (= eminentia capitata), shape in ventral view: (0) round; (1) angular (flattened lateral side); (2) horizontally oval (flattened on lateral and medial sides). (J)
5) Humerus, humeral ball, folds: (0) none; (1) oblique fold on the lateral side; (2) semi-circular fold.(J)
6) Humerus, humeral ball, inverted V-shaped depression in lateral view: (0) absent; (1) present. (J)
7) Humerus, humeral ball shape in medial view: (0) round; (1) oval. (J)
8) Humerus, humeral ball orientation in medial view: (0) straight; (1) downward oriented; (2) upward oriented. (J)
9) Humerus, lateral epicondyle, size: (0) relatively small (~½ of the humeral ball), not reaching distal margin of the humeral ball, *Strabomantis anomalus*; (1) moderately large, not surpassing distal margin of the humeral ball, *Leptodactylus validus*; (2) large, reaching or surpassing the distal margin of the humeral ball, *Pipa parva*. (GT21:238) (J*)
10) Humerus, lateral epicondyle, lateral projection: (0) pressed against the humeral ball, not projected laterally, *Phyzelaphryne miriamae*; (1) slightly projected laterally, *Adelophyrne gutturosa*; (2) strongly projected laterally, *Strabomantis anomalus*. (GT21:238) (J*)
11) Humerus, medial epicondyle, size: (0) relatively small (~½ of the humeral ball), not reaching distalmargin of the humeral ball, *Strabomantis anomalus*; (1) moderately large, not surpassing distal margin of the humeral ball, *Disasporus diastema*; (2) large, reaching or surpassing the distal margin of the humeral ball, *Leptodactylus validus* (GT21:239) (J*)
12) Humerus, medial epicondyle, medial projection: (0) pressed against the humeral ball, not projected medially, *Niceforonia araiodactyla*; (1) slightly projected medially, *Adelophryne gutturosa*; (2) strongly projected medially, *Osteocephalus taurinus*. (GT21:239)(J*)
13) Humerus, medial (ulnar) epicondyle, orientation in medial view: (0) pronounced angle with the diaphysis (at the level of the proximal end of the humeral ball); (1) Smooth angle (almost straight) with the diaphysis. (J)
14) Humerus, medial (ulnar) epicondyle, distal extremity, shape: (0) rounded; (1) flat; (2) concave. (J)

15) Humerus, medial (ulnar) epicondyle, oval depression in medial view: (0) absent; (1) present. (J)
16) Humerus, medial epicondyle ridge, relative position: (0) close from the humeral ball (ventrally oriented medial epicondyle); (1) distant from the humeral ball (dorsally-oriented medial epicondyle). (J)
17) Humerus, lateral (radial) epicondyle groove, shape: (0) shallow; (1) deep with an enlarged extremity; (2) deep with a V-shaped extremity and marked ridges. (J)
18) Humerus, lateral epicondyle shape in lateral view: (0) flattened; (1) forming a ridge. (J)
19) Humerus, lateral epicondyle shape in ventral view: (0) irregular; (1) angular (laterally extended); (2) almost vertically aligned with the proximo-distal axis. (J)
20) Humerus, medial epicondylar crest: (0) absent; (1) present, moderately to well developed. (G16:128)
21) Humerus, lateral epicondylar crest: (0) absent; (1) present, moderately to well developed. (J)
22) Humerus, ventral fossa: (0) shallow; (1) deep. (J)
23) Ilium, shaft, shape of the distal cross-section: (0) circular or nearly so; (1) horizontally oval, ilial shaft fairly compressed dorsoventrally; (2) flattened, ilial shaft much compressed dorsoventrally; (3) vertically oval, ilial shaft compressed mediolaterally; (4) kidney-shaped, almost circular but compressed dorsomedially. (GT21:244)
24) Ilium, shaft, length (relative to the height of the acetabular fossa): (0) short (around 5 times or less); (1) moderately long (around 6 times); (2) very long (clearly more than 6 times). (GT21:245)
25) Ilium, shaft, general aspect in acetabular view: (0) strongly and evenly curved along its length; (1) slightly to moderately curved, evenly curved along its length; (2) nearly straight along most ofits length; (3) distinctly curved proximally, but nearly straight distally. (GT21:246)
26) Ilium, dorsal prominence, relative height with respect to that of the acetabular fossa (DPH/AH; see Báez et al., 2012): (0) very low (DPH/AH < 0.1); (1) low to moderately high (DPH/AH between 0.1–0.7); (2) very high (DPH/AH > 0.7). (BGT12:60)
27) Ilium, dorsal prominence, shape in lateral profile: (0) bell-shaped, symmetrical, or nearly so withboth anterior and posterior margins gently sloping; (1) rectangular-shaped, symmetrical or nearly so with both anterior and posterior margins steep; (2) clearly asymmetrical with a posterior convex slope and anterior margin steep and slightly concave; (3) flat, not higher than the dorsal crest, *Adelophryne gutturosa*. (BGT12:61) (J*)
28) Ilium, dorsal prominence, orientation in dorsal aspect: (0) not inclined, vertically directed; (1) inclined medially; (2) inclined laterally. (BGT12:62)
29) Ilium, dorsal prominence, relative position of its apex with respect to the anterior margin of acetabular fossa: (0) clearly posterior; (1) approximately same level; (2) clearly anterior, on the ilial shaft. (BGT12:63)
30) Ilium, dorsal protuberance: (0) inconspicuous; (1) conspicuous. (BGT12:64)
31) Ilium, dorsal protuberance, shape: (0) elongate, projecting laterally; (1) nearly rounded, projecting laterally; (2) globose, projecting dorsolaterally; (3) quadrangular or tear-shape, projecting dorsolaterally, *Eleutherodactylus karlschmidti*; (4) ridge-like, projecting laterally, *Edalorhina perezi*. (BGT12:65) (J*)
32) Ilium, dorsal prominence/protuberance, origin of *m. gluteus magnus* relative to the level ofthe anterior margin of the acetabular fossa: (0) clearly posterior; (1) around this level; (2)

surpassing this level. (GT21:250)

33) Ilium, accessory knob for *m. iliofibularis-iliofemoralis*: (0) indistinct; (1) distinct. (GT21:251)
34) Ilium, spiral groove on shaft: (0) absent; (1) present. (B13:64)
35) Ilium, dorsal crest: (0) inconspicuous; (1) present as a low ridge; (2) well developed as a flange (wider than one half of the shaft width). (BGT12:66)
36) Ilium, dorsal crest, longitudinal extension relative to ilial shaft length: (0) restricted to distal halfof the ilial shaft; (1) extends along the anterior three fourths of the ilial shaft; (2) extends lengthwise or nearly so; (3) restricted to the proximal part of the ilial shaft. (BGT12:67)
37) Ilium, dorsal crest, orientation: (0) directed dorsally; (1) directed dorsolaterally; (2) directed laterally; (3) directed dorsomedially, *Eleutherodactylus karlschmidti*. (BGT12:68) (J*)
38) Ilium, dorsal crest depression: (0) absent; (1) present, slightly concave depression on the dorsal crest between the proximal portion of ilial shaft and the dorsal prominence. (J)
39) Ilium, lateral oblique ridge: (0) absent; (1) present. (BGT12:69)
40) Ilium, interilial scar: (0) inconspicuous; (1) ample but restricted to the ventral part of ilia; (2) ample both ventrally and dorsally. (BGT12:70)
41) Ilium, angle between the margin of the ventral acetabular expansion and the ventral margin of the ilial shaft in acetabular view: (0) acute; (1) nearly straight; (2) obtuse. (BGT12:71)
42) Ilium, dorsal acetabular expansion, lateral exposure in acetabular view: (0) broad; (1) narrow butdistinct; (2) minimal, inconspicuous. (BGT12:72)
43) Ilium, dorsal acetabular expansion, orientation: (0) posterodorsally, strong posterior vector, weak medial vector; (1) dorsomedially, weak dorsal and posterior vectors; (2) dorsally, strong dorsal vector, weak posterior and medial vectors. (GT21:248)
44) Ilium, supraacetabular fossa: (0) indistinct or shallow; (1) well distinct, deep. (GT21:252)
45) Ilium, preacetabular fossa: (0) indistinct or shallow; (1) well distinct, deep. (GT21:252)
46) Ilium, preacetabular zone in acetabular view: (0) not exposed; (1) narrow; (2) moderately broad; (3) broad. (GT21:254)
47) Ilium, proximal medial ridge: (0) absent; (1) present. (J)
48) Ilium, medial oblique groove: (0) absent; (1) present. (GT21:130)
49) Ilium, acetabular fossa, bony dorsal margin: (0) acetabular fossa merging with dorsal acetabular expansion; (1) poorly delimited by a shallow, rounded rim; (2) well delimited by a protruding, sharp rim, but only posterodorsally; (3) well delimited by a continuous protruding sharp rim. (GT21: 247)
50) Ilium, relation with ischium: (0) not fused; (1) fused to each other. (BGT12:73)
51) Ischium, shape of the posterior wall of the acetabulum in dorsal view: (0) slightly concave; (1) deeply concave. (BGT12:74)
52) Ischium, size in lateral view: (0) short, *Dendrobates tinctorius*; (1) long, *Leptodactylus validus*. (B13:68) (J*)
53) Ischium, shape in lateral view: (0) irregular outline, *Brachycephalus ephippium*; (1) semicircular outline, *Eleutherodactylus karlschmidti*; (2) outline rectangular dorsally and semicircular ventrally with a smooth transition, *Oreobates quixensis*; (3) outline rectangular dorsally and semicircular ventrally with a steep transition, *Pristimantis duellmani*; (4) outline rectangular, strongly protruded posterodorsally with a straight posteroventral margin, *Pipa parva*. (B13:68) (J*)

Table S3. Fossil CT-scan information

Inv. nr.	Locality	Skeleton Unit	Morphotype	MorphoMuseuM Access links	Resolution (mm)	Voltage (kv)	Amperage (µa)	Watts (W)
MUSM 4746	CTA-27	Humerus	1	https://morphomuseum.com/specimenfiles/send-file-specimenfile/1231/5b06efb6	0.00516367	80	60	N/A
MUSM 4747	CTA-27	Humerus	1	https://morphomuseum.com/specimenfiles/send-file-specimenfile/1232/dc251842	0.0058129	70	71	N/A
MUSM 4748	CTA-27	Humerus	1	https://morphomuseum.com/specimenfiles/send-file-specimenfile/1233/f1acefb7	0.0058129	70	71	N/A
MUSM 4755	CTA-27	Humerus	2	https://morphomuseum.com/specimenfiles/send-file-specimenfile/1234/d37a0463	0.00516367	80	60	N/A
MUSM 4756	CTA-29	Humerus	2	https://morphomuseum.com/specimenfiles/send-file-specimenfile/1235/d2decd40	0.0058141	70	71	N/A
MUSM 4757	CTA-61	Humerus	2	https://morphomuseum.com/specimenfiles/send-file-specimenfile/1236/a033c48b	0.00581419	70	71	N/A
MUSM 4761	CTA-27	Humerus	3	https://morphomuseum.com/specimenfiles/send-file-specimenfile/1237/f205aeef	0.0058129	70	71	N/A
MUSM 4763	CTA-27	Humerus	3	https://morphomuseum.com/specimenfiles/send-file-specimenfile/1238/d1021c57	0.0058129	70	71	N/A
MUSM 4765	CTA-27	Humerus	3	https://morphomuseum.com/specimenfiles/send-file-specimenfile/1239/dfe0e421	0.0058129	70	71	N/A
MUSM 4766	CTA-32	Humerus	3	https://morphomuseum.com/specimenfiles/send-file-specimenfile/1240/3dd26a09	0.00581462	70	71	N/A
MUSM 4775	CTA-27	Humerus	4	https://morphomuseum.com/specimenfiles/send-file-specimenfile/1241/e8874bb0	0.0058129	70	71	N/A
MUSM 4776	TMB-01	Humerus	5	https://morphomuseum.com/specimenfiles/send-file-specimenfile/1242/94e2b466	0.00581362	70	71	N/A
MUSM 4788	CTA-27	Ilium	A	https://morphomuseum.com/specimenfiles/send-file-specimenfile/1243/9d6369af	0.0058128	70	71	N/A
MUSM 4789	CTA-27	Ilium	A	https://morphomuseum.com/specimenfiles/send-file-specimenfile/1244/c14b25d6	0.0058129	70	71	N/A
MUSM 4790	CTA-27	Ilium	A	https://morphomuseum.com/specimenfiles/send-file-specimenfile/1245/73903b11	0.00516367	80	60	N/A
MUSM 4792	CTA-27	Ilium	B	https://morphomuseum.com/specimenfiles/send-file-specimenfile/1246/69746750	0.0058129	70	71	N/A
MUSM 4793	CTA-47	Ilium	C	https://morphomuseum.com/specimenfiles/send-file-specimenfile/1247/21b68462	0.00497596	29	2	N/A
MUSM 4794	CTA-27	Ilium	C	https://morphomuseum.com/specimenfiles/send-file-specimenfile/1249/6ebc79d0	0.0058129	70	71	N/A
MUSM 4795	CTA-27	Ilium	D	https://morphomuseum.com/specimenfiles/send-file-specimenfile/1250/8cba1b90	0.0058129	70	71	N/A
MUSM 4796	CTA-27	Ilium	E	https://morphomuseum.com/specimenfiles/send-file-specimenfile/1251/10758b66	0.0058129	70	71	N/A
MUSM 4797	CTA-29	Ilium	E	https://morphomuseum.com/specimenfiles/send-file-specimenfile/1252/08fea976	0.0058141	70	71	N/A

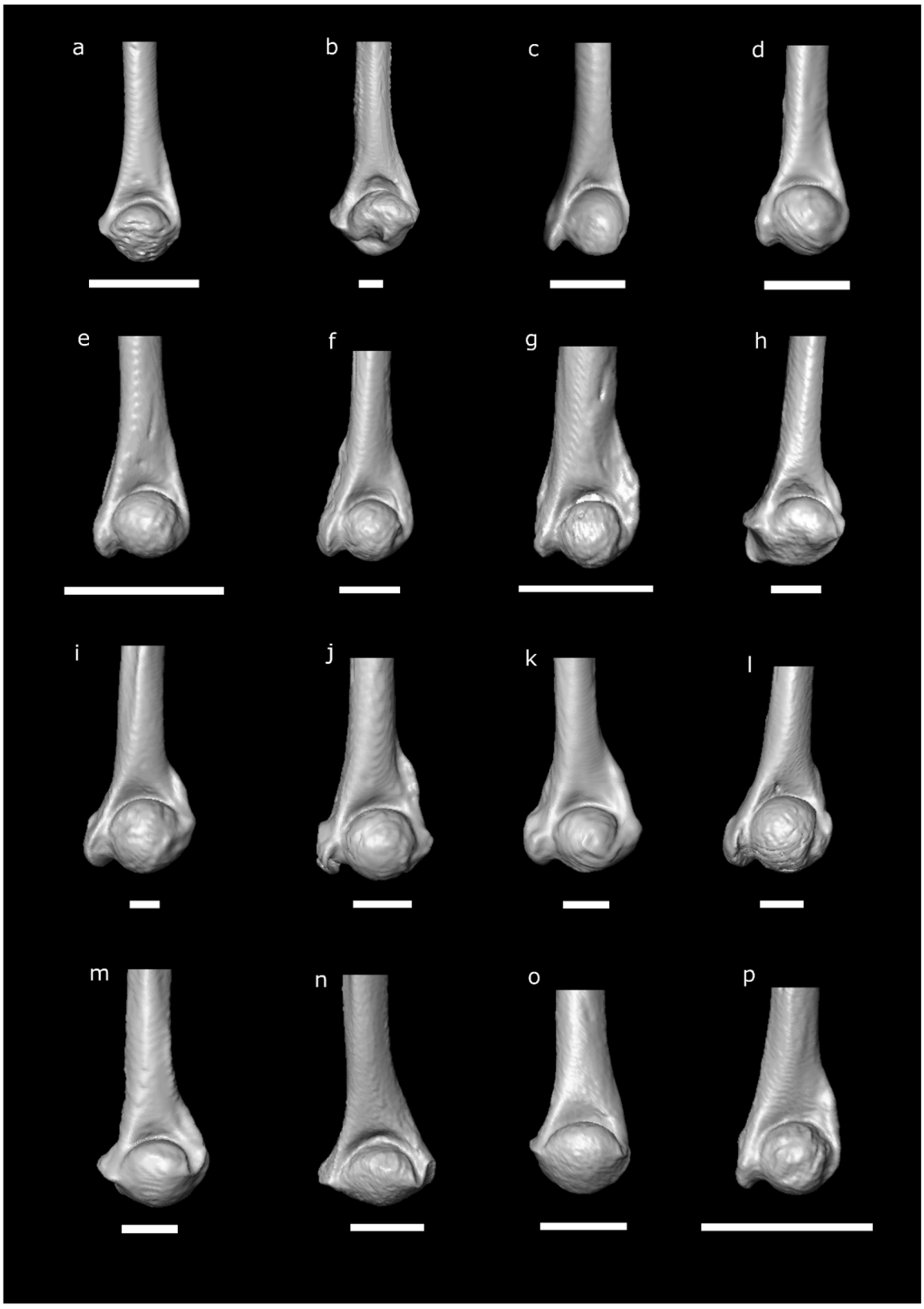
a
b
c
d
e
f
g
h
i
j
k
l
m
n
o
p

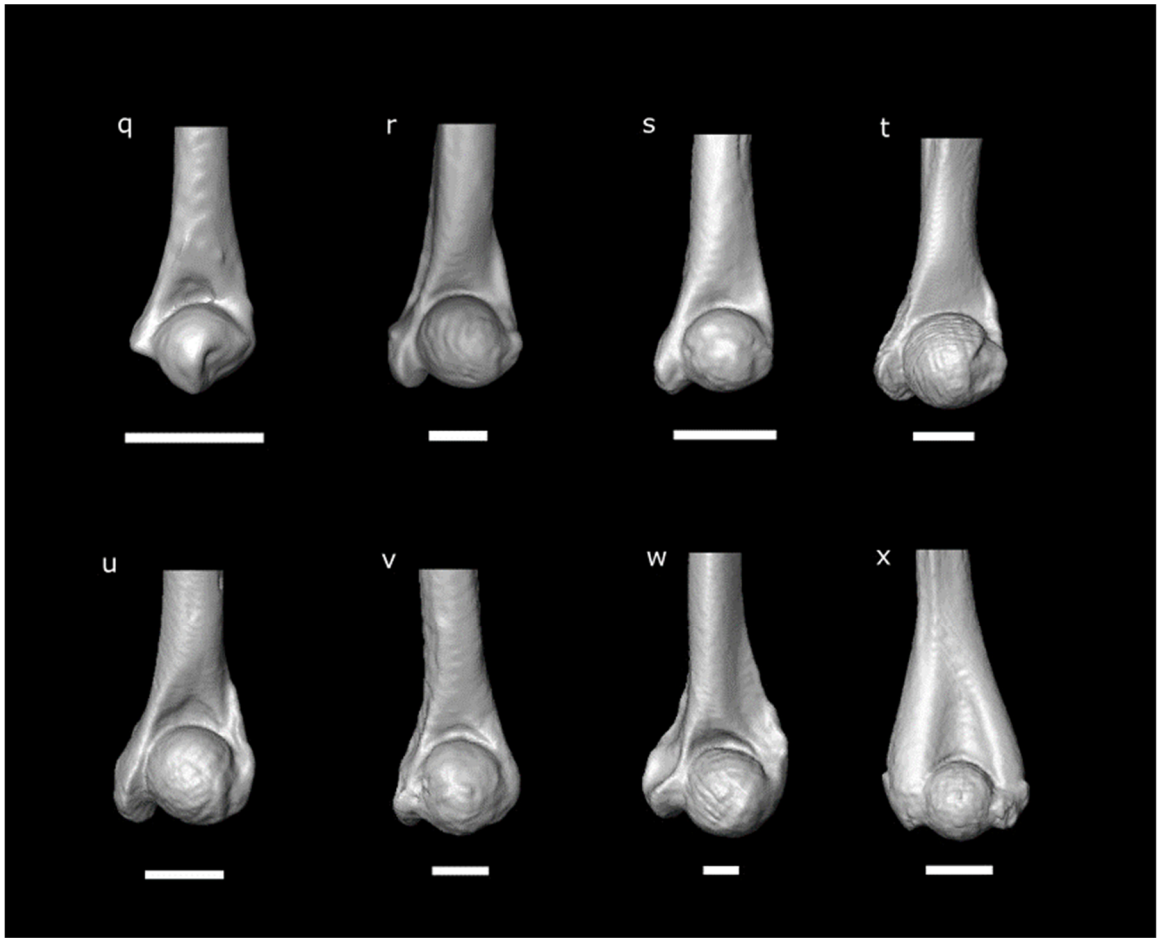

FIG S1. Humeri of extant Neotropical anurans. Left humeri in ventral view of: (a) *Ceuthomantis smaragdinus*; (b) *Eleutherodactylus karlschmidti*; (c) *Eleutherodactylus atkinsi*; (d) *Diasporus diastema;* (e) *Phyzelaphryne miriamae*; (f) *Adelophryne gutturosa*; (g) *Brachycephalus ephippium*; (h) *Haddadus binotatus*; (i) *Craugastor escoces*; (j) *Pristimantis vinhai*; (k) *Pristimantis duellmani*; (l) *Oreobates quixensis*; (m) *Strabomantis anomalus*; (n) *Strabomantis biporcatus*; (o) *Niceforonia araiodactyla*; (p) *Noblella myrmecoides* ©President and Fellows of Harvard College; (q) *Barycholos pulcher*; (r) *Leptodactylus validus*; (s) *Adenomera andreae*; (t) *Pleurodema nebulosum*; (u) *Edalorhina perezi*; (v) *Dendrobates tinctorius*; (w) *Osteocephalus taurinus*; (x) *Pipa parva*. Scale bars represent 1 mm.


a
b
c
d
e
f
g
h
i
j
k
l

FIG S2. Ilia of extant Neotropical anurans. Right ilia in lateral view of: (a) *Ceuthomantis smaragdinus*; (b) *Eleutherodactylus karlschmidti*; (c) *Eleutherodactylus atkinsi*; (d) *Diasporus diastema*; (e) *Phyzelaphryne miriamae*; (f) *Adelophryne gutturosa*; (g) *Brachycephalus ephippium*; (h) *Haddadus binotatus*; (i) *Craugastor escoces*; (j) *Pristimantis duellmani*; (k) *Oreobates quixensis*; (l) *Pristimantis vinhai*; (m) *Strabomantis anomalus*; (n) *Strabomantis biporcatus*; (o) *Niceforonia araiodactyla*; (p) *Noblella myrmecoides* ©President and Fellows of Harvard College; (q) *Barycholos pulcher*; (r) *Leptodactylus validus*; (s) *Adenomera andreae*; (t) *Pleurodema nebulosum*; (u) *Edalorhina perezi*; (v) *Dendrobates tinctorius*; (w) *Osteocephalus taurinus*; (x) *Pipa parva.* Scale bars represent 1 mm.

4) Humerus, humeral ball (= eminentia capitata), shape in ventral view: (0) round; (1) angular (flattened lateral side); (2) horizontally oval (flattened on lateral and medial sides).

(0)
Osteocephalus taurinus

(1)
Barycholos pulcher

(1)
Strabomantis biporcatus

5) Humerus, humeral ball, folds: (0) none; (1) oblique fold on the lateral side; (2) semi-circular fold.

(0)
Osteocephalus taurinus

(1)
Adelophryne gutturosa

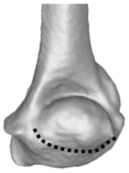

(2)
Haddadus binotatus

6) Humerus, humeral ball, inverted V-shaped depression in lateral view: (0) absent; (1) present

(0)
Osteocephalus taurinus

(1)
Adelophryne gutturosa

7) Humerus, humeral ball shape in medial view: (0) round; (1) oval. (J)

(0)
Osteocephalus taurinus

(1)
Strabomantis anomalus

8) Humerus, humeral ball orientation in medial view: (0) straight; (1) downward oriented; (2) upward oriented

(0)
Osteocephalus taurinus

(1)
Barycholos pulcher

(2)
Strabomantis anomalus

13) Humerus, medial (ulnar) epicondyle, orientation in medial view: (0) pronounced angle with the diaphysis (at the level of the proximal end of the humeral ball); (1) Smooth angle (almost straight) with the diaphysis.

(0)
Eleutherodactylus atkinsi

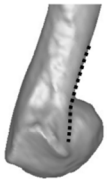

(1)
Strabomantis anomalus

14) Humerus, medial (ulnar) epicondyle, distal extremity, shape: (0) rounded; (1) flat; (2) concave.

(0)
Eleutherodactylus atkinsi

(1)
Osteocephalus taurinus

(2)
Strabomantis anomalus

15) Humerus, medial (ulnar) epicondyle, oval depression in medial view: (0) absent; (1) present.

(0)
Adenomera andreae

(1)
Edalorhina perezi

16) Humerus, medial epicondyle ridge, relative position: (0) close from the humeral ball (ventrally oriented medial epicondyle); (1) distant from the humeral ball (dorsally-oriented medial epicondyle).

(0)
Eleutherodactylus atkinsi

(1)
Ameerega trivittata

17) Humerus, lateral (radial) epicondyle groove, shape: (0) shallow; (1) deep with an enlarged extremity; (2) deep with a V-shaped extremity and marked ridges.

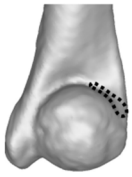

(0)
Adenomera andreae

(1)
Eleutherodactylus atkinsi

(2)
Strabomantis biporcatus

18) Humerus, lateral epicondyle shape in lateral view: (0) flattened; (1) forming a ridge.

(0) *Osteocephalus taurinus* (1) *Adelophryne gutturosa*

19) Humerus, lateral epicondyle shape in ventral view: (0) irregular; (1) angular (laterally extended); (2) almost vertically aligned with the proximo-distal axis

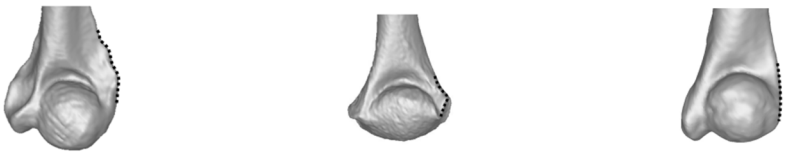

(0) *Osteocephalus taurinus* (1) *Strabomantis biporcatus* (2) *Adenomera andreae*

21) Humerus, lateral epicondylar crest: (0) absent; (1) present, moderately to well developed.

(0) *Ameerega trivittata* (1) *Osteocephalus taurinus*

22) Humerus, ventral fossa: (0) shallow; (1) deep.

(0) *Pleurodema nebulosa* (1) *Osteocephalus taurinus*

38) Ilium, dorsal crest depression: (0) absent; (1) present, slightly concave depression on the dorsal crest between the proximal portion of ilial shaft and the dorsal prominence.

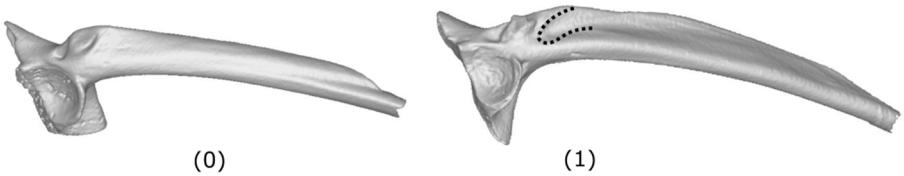

(0) *Eleutherodactylus karlschmidti* (1) *Strabomantis biporcatus*

43) Ilium, proximal medial ridge: (0) absent; (1) present. (J)

(0) *Osteocephalus taurinus* (1) *Eleutherodactylus atkinsi*

FIG S3. New characters considered in this study. Each character state is exemplified by an extant Neotropical species.